Alexandra Jahn[1, 2], L. Bruno Tremblay[1, 3], Robert Newton[3], Marika M. Holland[4], Lawrence A. Mysak[1], Igor A. Dmitrenko[5]

A tracer study of the Arctic Ocean's liquid freshwater export variability

An edited version of this paper was published by AGU in the Journal of Geophysical Research - Ocean, Vol. 115, C07015, doi:10.1029/2009JC005873.

I. A. Dmitrenko, Leibniz Institute of Marine Sciences, University of Kiel, Wischhofstrasse 1-3, D-24148 Kiel, Germany.

M. M. Holland, National Center for Atmospheric Research, PO Box 3000, Boulder, CO 80307-3000, USA.

A. Jahn, L. B. Tremblay, L. A. Mysak, Department of Atmospheric and Oceanic Sciences, McGill University, 805 Sherbrooke Street West, Montréal, Québec, H3A 2K6, Canada. (alexandra.jahn@mail.mcgill.ca)

R. Newton, Lamont-Doherty Earth Observatory, 61 Route 9W, P.O. Box 1000, Palisades, NY 10964, USA.

[1]Department of Atmospheric and Oceanic Sciences, McGill University, Montréal, Québec, Canada

Abstract. We present an analysis of the variability of the liquid Arctic freshwater (FW) export, using a simulation from the Community Climate System Model Version 3 (CCSM3) that includes passive tracers for FW from different sources. It is shown that the FW exported through the western Canadian Arctic Archipelago (CAA) comes mainly from the Pacific and from North American runoff. The variability of the FW export from both of these sources is generally in phase, due to the strong influence of variations of the velocity anomaly on the CAA FW export variability. The velocity anomaly in the CAA is in turn mainly governed by variations in the large-scale atmospheric circulation (i.e., the Arctic Oscillation). In Fram Strait, the FW export is mainly composed of Eurasian runoff and FW of Pacific origin. The variabil-

[2]Now at National Center for Atmospheric Research, Boulder, Colorado, USA

[3]Lamont-Doherty Earth Observatory of Columbia University of New York, Palisades, New York, USA

[4]National Center for Atmospheric Research, Boulder, Colorado, USA

[5]Leibniz Institute of Marine Sciences at University of Kiel (IFM-GEOMAR), Kiel, Germany

ity of the Fram Strait FW export is governed both by changes in the velocity and in the FW concentration, and the variability of the FW concentration from the two largest sources is not in phase. The Eurasian runoff export through Fram Strait depends strongly on the release of FW from the Eurasian shelf, which occurs during years with an anticyclonic circulation anomaly (negative Vorticity index) and takes 3 years to reach Fram Strait after leaving the shelf. In contrast, the variability of the Pacific FW export through Fram Strait is mainly controlled by changes in the Pacific FW storage in the Beaufort Gyre, with an increased export during years with a cyclonic circulation anomaly (positive Vorticity index).

1. Introduction

The upper Arctic Ocean contains a large volume of freshwater (FW) relative to the mean salinity of the Arctic Ocean, due to the large amount of river runoff it receives and the inflow of low salinity Pacific surface water through Bering Strait. This FW storage of 84,000 km^3 is about 10 times larger than the annual FW input or export from the Arctic [*Serreze et al.*, 2006]. A release of part of this FW to the North Atlantic through Fram Strait and the Canadian Arctic Archipelago (CAA) has the potential to influence the strength of the Atlantic meridional overturning circulation (MOC) [e.g., *Aagaard et al.*, 1985; *Aagaard and Carmack*, 1989; *Weaver et al.*, 1993; *Häkkinen*, 1995; *Lohmann and Gerdes*, 1998; *Holland et al.*, 2001; *Rennermalm et al.*, 2006, 2007; *Arzel et al.*, 2008], provided it can reach the interior Labrador and/or Greenland seas where deep water formation takes place [e.g., *Myers*, 2005; *Gerdes et al.*, 2005; *Jones et al.*, 2008; *Nilsson et al.*, 2008; *Condron et al.*, 2009; *Dodd et al.*, 2009]. Within the Arctic Ocean, changes in the distribution of FW can lead to changes in the stratification of the water column [*Schlosser et al.*, 2002] and to a regional disappearance of the cold halocline [*Steele and Boyd*, 1998; *Martinson and Steele*, 2001; *Björk et al.*, 2002; *Schlosser et al.*, 2002; *Newton et al.*, 2008]. This has implications for the ice/ocean heat exchange and the state of the Arctic sea ice [*Martinson and Steele*, 2001]. Furthermore, the river water entering the Arctic Ocean also carries nutrients and contaminants (e.g., lead, pesticides, and radionuclides [e.g., *AMAP*, 1998; *Harms et al.*, 2000; *Macdonald et al.*, 2005]), due to agricultural and industrial activities in their drainage basins. Changes in the distribution of FW from different sources therefore also affect the nutrient and contaminant transport within and from the Arctic

Ocean, with important implications for the marine environment [e.g., *Macdonald et al.*, 2003].

Due to a lack of long term observations, the variability of the liquid FW export from the Arctic Ocean is not well understood. Previous work has shown that changes in the large-scale atmospheric circulation affect the position and size of the Beaufort Gyre, which leads to changes in the distribution of FW in the Arctic Ocean due to changes in the Ekman transport [*Hunkins and Whitehead*, 1992; *Proshutinsky et al.*, 2002; *Zhang et al.*, 2003; *Häkkinen and Proshutinsky*, 2004; *Karcher et al.*, 2005; *Newton et al.*, 2006; *Köberle and Gerdes*, 2007; *Condron et al.*, 2009; *Proshutinsky et al.*, 2009; *Jahn et al.*, 2010a]. Whether these changes in Ekman transport in the Beaufort Sea are also the main reason for changes in the liquid FW export from the Arctic Ocean is still a topic of active research [*Zhang et al.*, 2003; *Karcher et al.*, 2005; *Köberle and Gerdes*, 2007; *Arzel et al.*, 2008; *Condron et al.*, 2009; *Lique et al.*, 2009; *Jahn et al.*, 2010a]. The results from these recent studies, however, do not yet agree on the mechanisms underlying the variability of the FW export, with some suggesting a large influence of atmospheric forcing on the FW export [*Zhang et al.*, 2003; *Karcher et al.*, 2005; *Koenigk et al.*, 2007; *Condron et al.*, 2009; *Jahn et al.*, 2010a], while others find no clear response to the atmospheric forcing [*Köberle and Gerdes*, 2007; *Arzel et al.*, 2008; *Lique et al.*, 2009].

Given that the FW exported from the Arctic comes from many different sources, with different pathways and different travel times to Fram Strait and the CAA, the variability of the liquid FW export is a complex combination of the variability of FW from all these sources. In fact, observations show that the concentrations of FW from different sources in Fram Strait show large variations from year to year [e.g., *Falck et al.*, 2005; *Rabe et al.*,

2009; *Dodd and Hansen*, 2009]. Furthermore, observations also indicate that a decrease in the FW concentration from one source is often compensated by FW from a different source [*Rabe et al.*, 2009; *Dodd and Hansen*, 2009], so that the total FW export is not in phase with the FW export from individual sources. In order to understand the dynamics that lead to changes in the liquid FW export from the Arctic, the variability of FW from different sources needs to be investigated separately.

Salinity alone is not sufficient to separate the FW export into contributions from different sources; thus, other tracers are needed. Most ocean models, however, do not include the geochemical tracers that are used to separate water samples into different water masses (e.g., δ^{18}O, total alkalinity, nitrate, phosphate, silicate, dissolved barium). As a substitute, passive dye tracers have been used to track runoff and/or Pacific water in some model studies [e.g., *Weatherly and Walsh*, 1996; *Nazarenko et al.*, 1998; *Maslowski et al.*, 2000; *Karcher and Oberhuber*, 2002; *Harms et al.*, 2000; *Newton et al.*, 2008; *Gao et al.*, 2009]. These tracers, however, have never been used to specifically study the FW export variability. Furthermore, FW contributions from sea-ice melt and sea-ice formation have not previously been accounted for in models, so that it has not been possible to separate the FW export into FW from all significant sources in model simulations.

The main purpose of this article is to fill this gap in the literature by studying the mechanisms that lead to the interannual variability of FW export from individual sources. To this end, we include passive tracers for FW from all Arctic sources in the ocean model of the CCSM3. The results presented in this article show how and why the export of FW from different sources varies from year to year, and how the variability of FW from the different sources leads to the total variability of the liquid FW export from the Arctic. In

a complementary study, seasonal changes in the Fram Strait export are described in *Jahn et al.* [2010b].

The outline of this article is as follows: The model simulation is described in section 2, and the simulated FW budget, the contribution of FW from different sources and the residence times of FW from different sources are presented in section 3. In section 4 we analyze the interannual variability of the FW export from individual sources. The atmospheric forcing of the FW export variability is described in section 5. Conclusions and a summary are presented in section 6.

2. Methods

2.1. Model

The CCSM3 is a fully coupled general circulation model, which conserves energy and mass and does not use flux adjustments. The atmospheric component of the CCSM3 is the Community Atmosphere Model version 3 [CAM3; *Collins et al.*, 2004, 2006b]. This model has a spectral truncation of T85 (about 1.4°× 1.4°). The ocean component of the CCSM3 is based on the Parallel Ocean Program version 1.4.3 [POP; *Smith and Gent*, 2004]. It has a free surface, includes the Gent-McWilliams [*Gent and McWilliams*, 1990] and K-profile [*Large et al.*, 1994] parametrizations of mixing, and uses a 3rd-order upwind advection scheme with a leapfrog time step. It has a 1° rotated orthogonal grid, in which the North Pole is displaced to Greenland, and 40 vertical levels, ranging from a thickness of 10 m at the surface to 250 m at depth. Surface processes that lead to a FW flux (runoff, precipitation, evaporation, sea-ice melt, and sea-ice formation) are added to the ocean through virtual salt fluxes, using a reference salinity of 34.7, which is the global average salinity. The sea-ice component of the CCSM3 is the Community Sea

Ice Model version 5 [CSIM5; *Briegleb et al.*, 2004], which is a dynamic-thermodynamic model that includes a subgrid-scale ice thickness distribution [*Thorndike et al.*, 1975], energy conserving thermodynamics [*Bitz and Lipscomb*, 1999], and elastic-viscous-plastic (EVP) dynamics [*Hunke and Dukowicz*, 1997]. The land component of the CCSM3 is the Community Land Model version 3 [CLM3; *Oleson et al.*, 2004; *Dickinson et al.*, 2006]. Except for the river routing scheme, which has a 0.5° resolution, CLM3 uses the same resolution as the atmospheric model. A more detailed description of the CCSM3 is given in *Collins et al.* [2006a].

2.2. Tracers

To follow the path of liquid Arctic FW from different sources, we included 12 passive tracers in the POP ocean model, accounting for all of the FW sources in the Arctic Ocean. These include tracers for FW fluxes from river runoff into the different Arctic shelf seas, sea-ice melt, sea-ice formation, precipitation and evaporation over open water areas, and for the FW inflow from the Pacific and Atlantic oceans. All tracers are conservative, and their time evolution is described by the same advection/diffusion equations as used for salinity and temperature. For consistency with the virtual salt fluxes in the model, the tracers are added relative to the same reference salinity (34.7), and all FW fluxes in this study are also calculated relative to 34.7. The difference in the FW fluxes associated with this choice of reference salinity compared to the commonly used reference salinity of 34.8 [*Aagaard and Carmack*, 1989] is small, and is quantified in section 3.

Tracers were added as surface fluxes for (i) river runoff into the different shelf seas (Barents, Kara, Laptev, East Siberian, Beaufort, and Lincoln seas), (ii) the precipitation/evaporation into/from the open-water fraction of the Arctic Ocean, and (iii) the FW

flux due to sea-ice melt and sea-ice formation within the Arctic Ocean. Note that the river discharge field in the CCSM3 is distributed over the shelf seas instead of entering in the ocean grid box nearest to the coast (see Fig. 1 for the input patches for the runoff and the borders of shelf seas used for the runoff tracers). This spreading of the runoff is necessary because the simulated ocean circulation over the shelves is sluggish compared with observations [*Newton et al.*, 2008], and runoff would otherwise accumulate at the river mouths. The sea-ice formation tracer keeps track of the amount of FW removed from the surface ocean when sea ice forms (which has a salinity of 4 in the CCSM3). The melt tracer accounts for the FW flux due to melting sea ice. It also includes small contributions from the (i) runoff of rain that falls on the sea-ice, (ii) runoff of snow melt on the surface of the sea ice, and (iii) surface snow that falls into the water during sea-ice ridging. For the oceanic FW inflow into the Arctic Ocean through Bering Strait (Pacific FW tracer) and through Fram Strait and the Barents Sea Opening between Norway and Svalbard (Atlantic FW tracer), the tracers were added as interior source terms (see Fig. 1 for the definition of the ocean boundaries). The tracer input at these boundaries is equal to the FW flux that enters the Arctic Ocean through these straits, relative to the reference salinity of 34.7.

The runoff, precipitation, sea-ice melt, and Pacific FW tracers are positive because they add FW to the Arctic Ocean. The sea-ice formation and evaporation tracers, on the other hand, are negative because these processes remove FW from the water column. The Atlantic FW tracer can be either positive or negative, depending on the salinity of the FW inflow. However, except for the Norwegian Coastal current that carries FW into the Barents Sea, the salinity of the Atlantic inflow is generally larger than or equal to

the reference salinity, so that, on average, the Atlantic FW tracer is negative. Due to the presence of these negative FW tracers, the contribution of FW from individual sources can be more than 100% of the total FW.

To account for the recirculation of tracers, any FW tracer that enters the Arctic Ocean from the Greenland, Icelandic, and Norwegian (GIN) seas is subtracted from the Atlantic FW tracer that is added. The FW tracers therefore account for all the FW present in the Arctic Ocean surface water once steady-state has been reached. Note that the Atlantic FW tracer is mainly located below the halocline in the Arctic Ocean, which leads to a much longer spin-up time compared to the other tracers. As a result, the negative Atlantic FW tracer has not yet reached equilibrium in this simulation, and the sum of the FW tracers can therefore reach more than 100% of the FW calculated from the salinity (see section 2.3).

Due to stronger gradients in the individual FW tracer fields compared to the gradients in the salinity field, the diffusive tracer fluxes are larger than the diffusive salinity fluxes. This results in some differences between the FW distribution calculated from salinities and the FW distribution calculated from the sum of the FW tracers. One example is a too large Atlantic FW tracer concentration in the upper layers of the East Greenland Current (EGC), due to upward diffusive fluxes from the much higher concentration of Atlantic FW tracer at depth compared to the surface. At the same time, the other tracers penetrate deeper, due to downward diffusive fluxes. This has some effect on the calculated FW fluxes based on the FW tracers at Fram Strait, as discussed in section 3.1.

In observational data, geochemical tracers (e.g., salinity, δ^{18}O, silicate, total alkalinity, barium, phosphate, and nitrate) are used to separate the water mass into Pacific, Atlantic,

meteoric (runoff plus precipitation), and net sea-ice melt (NSIM) contributions. The NSIM is the sum of FW fluxes due to sea-ice melt and sea-ice formation, and it therefore gives the amount of net sea-ice melt in the history of a water mass. It is often negative, as on average sea-ice formation is larger than sea-ice melt within the Arctic Ocean, due to the sea-ice export. To compare our results with observational data, we also calculate the NSIM FW fraction from the simulation. However, as seen in section 4.2, the dynamics of the NSIM FW export sometimes cannot be understood without separating it into contributions from sea-ice melt and sea-ice formation. For this reason, we also discuss the sea-ice formation and sea-ice melt tracers when necessary. For simplicity, we also combine the precipitation and evaporation tracer into a net precipitation tracer in the following sections, except where the dynamics of the individual tracers are very different from the net.

2.3. Simulation

We perform a 140 year long simulation with constant atmospheric CO_2 concentrations. This run is initialized from the end of year 399 of the 1990 CCSM3 equilibrium simulation (simulation b30.009). This CCSM3 control integration is part of the Coupled Model Intercomparison Project, 3 (CMIP3) archive and was discussed in the IPCC-AR4 [*IPCC*, 2007]. The mean climate of the 1990 equilibrium simulation for the years 400–500, when equilibrium has been reached except for small changes in the deep ocean, is described in detail in *Collins et al.* [2006a]. It should be noted that the climate in this 1990 equilibrium simulation is warmer than the mean observed climate of the 20th century because it is in quasi-steady-state with the climate forcing. This results in a mean climate that is roughly comparable to the simulated mean climate of the early 21st century, with an intensified

hydrological cycle over the Arctic as well as thinner Arctic sea ice than in a 20th century simulation with the same model. We perform an equilibrium simulation, instead of a transient simulation for the 20th or 21st century, to isolate the effect of the atmospheric forcing on the liquid FW export variability, without any disturbances from changes in the liquid FW input into the Arctic associated with enhanced greenhouse gas forcing [see *Holland et al.*, 2006b].

The concentrations of the tracers in the Arctic Ocean increase rapidly during the first two decades of the simulation, with a more gradual increase in the third and fourth decade. Around simulation year 440, the tracers reach their spun-up state for all tracers except the Atlantic tracer (not shown), which takes well over 100 years to reach steady state because most of it is found below the halocline, where the renewal time is much longer than for the surface ocean. All results presented in the following are for simulation years 440 to 539 (100 years). Due to the still increasing Atlantic tracer concentration over the course of the simulation, the total Arctic FW export calculated from the sum of the FW tracers is on average 10% larger than the FW export calculated from salinity, as some salty water of Atlantic origin below the halocline is not yet "tagged" (see section 3.1).

3. Arctic FW budget

The simulated Arctic FW budget of the CCSM3 during the 20th century is discussed in detail by *Holland et al.* [2006b]. It was found to be in general agreement with the observational budget of *Serreze et al.* [2006], which is shown as third column in Table 1. The main difference between the CCSM3 FW budget and the observational FW budget is a larger simulated liquid FW export through Fram Strait and a smaller simulated liquid FW export through the CAA. The simulated river runoff is generally larger than

in observations, which in turn leads to fresher than observed Pacific water inflow through Bering Strait (a mean of 31.2 in the model versus 32.5 in observations). This means that the FW input into the Arctic is larger than observed, which leads to a larger than observed simulated FW export. Most of this FW export occurs through Fram Strait, as only one CAA channel in the location of Barrow Strait is open in the model; Nares Strait and the many other smaller channels in the CAA are closed, due to the model resolution (see Fig. 1). The simulated FW flux through the CAA is therefore only representative for the western CAA, and the simulated Fram Strait flux includes the FW flux through both Fram Strait [about 2400 km^3/yr, according to *Serreze et al.*, 2006] and Nares Strait [about 788 km^3/yr, according to *Münchow et al.*, 2006].

The FW budget calculated here (Table 1) is very similar to the one of *Holland et al.* [2006b], except for a larger liquid FW export through Fram Strait and a smaller sea-ice export. These changes are consistent with the warmer climate in the 1990-equilibrium simulation compared to the mean of the transient 20th century simulation of *Holland et al.* [2006b]. In addition, FW fluxes are calculated relative to a reference salinity of 34.7 here (as opposed to 34.8 in *Serreze et al.* [2006] and *Holland et al.* [2006b]), for reasons explained in section 2.2. This leads to a smaller liquid FW flux through Fram Strait and a larger liquid FW flux through the Barents Sea Opening (see Table 1 for details).

The oceanic transport through Fram Strait consists of the export of fresh and cold polar water in the EGC and the inflow of warm and salty water in the West Spitzbergen current. The variability of the simulated Fram Strait liquid FW transport is dominated by the outflowing branch ($r=0.98$; $p<0.05$ for all correlation coefficients given in this article), and most of the FW in Fram Strait is located above 247 m. Below 247 m the

outflow through Fram Strait is a source of FW for the Arctic, as the salinity of the deep outflow is larger than the reference salinity. The southward FW flux through Fram Strait is therefore larger in the top 247 m compared to that for the full depth (by 1804 km^3/yr). In the remainder of this article, we will investigate only the FW transport in the top 247 m that is directed out of the Arctic Ocean, as our main goal is to better understand the variability of the fresh polar water export from the Arctic. The exact choice of the integration depth, however, does not affect the general conclusions of this study. In the CAA, the simulated transport is always directed out of the Arctic and the section through the CAA is only 247 m deep at the deepest point. Consequently, this approach has no effect in the CAA.

3.1. Contributions from different sources to the FW export

By using the FW tracers, we can quantify the contribution of FW from each source to the total FW export (calculated from the salinity). These percentages are shown in Table 2. Averaged over the years 440-539 of the simulation, the FW tracers account for 94% of the Fram Strait FW export calculated from the simulated salinity in the upper 247 m, and 105% of the FW export through the CAA. In both cases the difference between the sum of the FW tracer exports and the FW export calculated from the salinity is mainly due to the contribution of the Atlantic FW tracer. In the CAA, the export of negative FW of Atlantic origin is still increasing at the end of the simulation because it has not yet reached its equilibrium. The negative Atlantic FW export is therefore not large enough to balance the positive FW from other sources, so that the sum of all tracers is larger than 100% (see section 2.2). In Fram Strait, on the other hand, the FW concentration based on the salinity is larger in the top 150 m than the FW concentration derived from the sum

of the FW tracers. This is due to a too large concentration of the Atlantic FW tracer in the top 150 m, due to upward diffusive fluxes of this tracer (see section 2.2). This error leads to an overall smaller FW export calculated from the FW tracers than from salinity if the FW fluxes are calculated over the upper 247 m only. Over the full depth, where the vertical distribution of the Atlantic tracer is not important, the FW flux calculated from the tracers makes up 111% of the Fram Strait FW export calculated from salinities, due to the still increasing concentration of the Atlantic tracer in the export at depth.

The simulated FW export through Fram Strait is mainly composed of sea-ice melt water (153%), river water (73%), and Pacific FW (48%), with a smaller contribution from precipitation (21%). Most (88%) of the river water exported through Fram Strait comes from Eurasia (see Table 2), and only 12% comes from North America (Beaufort and Lincoln seas (see Fig. 1), which will henceforth be referred to as runoff from North America). The export of negative FW from sea-ice formation (−167%), evaporation (−16%), and of salty Atlantic water (−18%) reduce the total FW flux. If we only consider NSIM (as done in observations), the largest contribution to the Fram Strait FW export comes from Eurasian runoff (64%) and Pacific FW (48%), and NSIM contributes only −14% of the Fram Strait FW export.

In the CAA, most of the FW exported comes from sea-ice melt (122%), followed by Pacific FW (59%), and river runoff (39%). The runoff is mainly (82%) of North America origin and contains only 18% of Eurasian runoff (see Table 2). Negative FW from sea-ice formation (−115%), evaporation (−4%), and Atlantic water (−3%) reduce the liquid FW export through the CAA. If we combine sea-ice melt and sea-ice formation, the

contribution of NSIM is 7% of the FW export, and the dominant sources of FW are Pacific FW (59%) and North American runoff (32%).

In this simulation, about 2/3 of the Pacific FW that enters the Arctic through Bering Strait leaves through Fram Strait, and 1/3 of it leaves through the CAA. About half of the simulated North American runoff that enters the Arctic leaves through CAA, and the rest through Fram Strait. The runoff from Eurasia on the other hand leaves the Arctic mainly (97%) through Fram Strait, with only 3% leaving through the CAA. Due to the closed Nares Strait in the CCSM3, the export of Pacific FW and North American runoff through Fram Strait is likely overestimated by the CCSM3. Observations show that the Nares Strait FW export is made up mainly of Pacific FW, with smaller contributions from North American and Eurasian runoff [*Jones et al.*, 2003]. Opening Nares Strait in the model should therefore decrease the concentration of the simulated Pacific FW and North American runoff in Fram Strait. It would also likely increase the Eurasian runoff export through the total CAA. As mentioned earlier, the discussion of the FW fluxes through the CAA in this study is therefore only applicable to the western CAA, and the simulated Fram Strait FW fluxes include the FW export through both Nares Strait and Fram Strait.

3.2. Comparison with observations

The simulated Eurasian runoff makes up only 0.9% of the volume export through the CAA, which agrees reasonably well with results from *Taylor et al.* [2003], who found no Eurasian river water in the western CAA. For Fram Strait, *Taylor et al.* [2003] found no evidence of Mackenzie water. This agrees with the very small contribution of only 0.2% Beaufort Sea runoff to the Fram Strait volume export, which is within the error estimate of the data [*Taylor et al.*, 2003]. The model shows a ratio of 2.3 : 1 between the long-term

mean meteoric FW export and the solid FW export due to the sea-ice export through Fram Strait, which compares well with the 2 : 1 ratio found by *Bauch et al.* [1995b] and *Meredith et al.* [2001]. The slight overestimation of meteoric water relative to the solid FW export is likely due to the smaller simulated sea-ice export than at present, associated with the thinner than observed sea ice in the warmer climate of this simulation. As noted above, some of the meteoric FW in Fram Strait should also leave through Nares Strait. The model simulates a large interannual variability of the Pacific FW export through Fram Strait, but the Pacific water fraction is never as small as reported by *Falck et al.* [2005] for 2004. This might be a consequence of the larger than observed Pacific FW input and/or of the closed Nares Strait. Overall, the model captures many features of the FW composition of the export well. This is also shown in *Jahn et al.* [2010b], where the simulated seasonal variability and spatial distribution of FW from different sources in Fram Strait are discussed.

3.3. Residence and transport times

The residence time of water in the Arctic (also called flushing time) is commonly calculated as the ratio between the storage of water from a given source and the mean annual input of water from that source. For the Arctic halocline, this calculation yields a residence time of around 10 years [e.g., *Östlund and Hut*, 1984]. This agrees well with the simulated residence time of 11 years for the FW in the top 247 m of the Arctic Ocean. River runoff is found to have a mean Arctic residence time of 11 years in the simulation, which agrees well with values of 11–15 years derived from observational and other model results [*Bauch et al.*, 1995a; *Prange and Gerdes*, 2006]. The simulated residence times vary for river runoff into the different shelf seas, from 20 years for river runoff into the

East Siberian Sea to 7 years for river runoff entering into the Kara and Lincoln Sea, with intermediate values of 14 years for the Barents Sea runoff, and 12 years for the Beaufort and Laptev Sea runoff. At 21 years, Pacific FW has the longest simulated residence time in the Arctic Ocean, which is due to the storage of a large portion of the Pacific FW in the Beaufort Gyre (see section 5). A long residence time of Pacific FW in the Arctic Ocean agrees with geochemical tracer observations, which yield an estimated residence time of 11 ± 4 years for Pacific water [*Yamamoto-Kawai et al.*, 2008].

The minimum advective transport time of FW from different sources to Fram Strait and the CAA can be estimated by examining the time it takes the tracers to first reach these straits at the beginning of the simulation. We find that Pacific FW first appears in Fram Strait after 6 years. North American runoff reaches Fram Strait after 7 years. Eurasian runoff is present in Fram Strait after 3 years, with Kara Sea runoff arriving first (after 3 years), followed by Laptev Sea and Barents Sea runoff after 4 years, and East Siberian runoff after 6 years. As these are minimum transit times, and observational estimates give mean residence and transit times, a direct comparison with observations is not possible. However, a minimum transit time for East Siberian runoff to Fram Strait on the order of 6 years is supported by observational estimates of the mean residence time of 3.5 ± 2 years for river water on the Eurasian shelves [*Schlosser et al.*, 1994] and a transport time of 2–3 years in the Transpolar Drift Stream (TDS) from the East Siberian shelf to Fram Strait [*Rutgers van der Loeff et al.*, 1995].

Pacific FW reaches the CAA after 4 years. Due to the proximity of the Mackenzie river discharge to the CAA location in the model, river water from North America is present in the CAA from the start. The first Eurasian runoff reaches the western CAA after 6 years.

This runoff originates from the East Siberian Sea, and is followed by Laptev and Kara Sea runoff (9 years), and by Barents Sea runoff (15 years). Transport times of Eurasian runoff to Nares Strait should be much shorter. Atlantic FW first appears in the CAA after 15 years, but contributes little to the outflow through the CAA.

4. Interannual variability of FW export from different sources

As seen in Fig. 2, the simulated FW export has a large interannual variability. The variability of the total FW export (black lines in Fig. 2) is caused by the sum of the variability of FW from different sources. In the CAA (Fig. 2b), the FW exports from the two largest sources, Pacific FW and North American runoff, are in phase and have a correlation of r=0.64. In Fram Strait (Fig. 2a), the FW export from the two largest FW sources, Eurasian runoff and Pacific FW, are not in phase and also do not have a simple lagged correlation.

The interannual variability of the FW export can be due to changes in the velocity and/or changes in the salinity of the outflow, which in turn can be driven by density gradients, sea surface height (SSH) gradients, and/or large-scale or local atmospheric circulation patterns. In addition, changes in the input of FW can either directly affect the FW export variability (with a certain lag) or accumulate in the Arctic over many years, which decouples the input anomaly from the export anomaly. In the following, we will investigate the mechanisms that cause the variability of the FW export from individual sources, in order to understand the variability of the FW export in Fram Strait and the CAA, as well as the differences between the two straits.

4.1. FW input versus FW storage changes

Although the long-term averaged FW inputs are balanced by FW exports, the simulated variability of the FW export from the Arctic is generally not correlated with changes in the FW inputs (black lines in Fig. 3). This means that the Arctic Ocean decouples the variability of the FW input and export by storing FW for variable lengths of time. A small exception is the Bering Strait FW inflow, which has a moderate influence on the simulated FW export variability (r=0.32 at a 4-year lag of the export behind the inflow; Fig. 3a).

The effect of interannual changes of the FW input on the variability of the FW storage in the Arctic Ocean differs strongly for FW from different sources (light grey lines in Fig. 3). Whereas the FW input from NSIM and net precipitation (and also from sea-ice formation, sea-ice melt, evaporation, and precipitation individually; not shown) has a large effect on the storage of FW from these sources in the Arctic, the variability of the FW input from runoff has only a very small effect on the storage of runoff in the Arctic Ocean. For the Pacific FW, changes in the inflow have some effect on the storage of Pacific FW in the Arctic, but much less than for NSIM and net precipitation. This means that temporal changes in the storage of runoff and Pacific FW in the Arctic Ocean are more strongly linked with the variability of the FW exchange with the North Atlantic than with the variability of their FW input. The Arctic storage of FW from NSIM and net precipitation on the other hand is influenced mainly by changes in their input.

4.2. FW concentration versus velocity anomalies

In order to investigate the contribution of velocity and FW concentration anomalies to the interannual variability of the FW export, we split the FW export (F_{FW}) into a

time-mean component and three time-varying terms:

$$F_{FW} = \langle C_{FW} \rangle \langle v_\perp \rangle + v'_\perp \langle C_{FW} \rangle + C'_{FW} \langle v_\perp \rangle + C'_{FW} v'_\perp, \quad (1)$$

where $v_\perp$ is the velocity component perpendicular to the strait and C_{FW} is the concentration of FW relative to the reference salinity. Primed variables stand for temporal anomalies and variables in brackets stand for time mean values. Accordingly, $\langle C_{FW} \rangle \langle v_\perp \rangle$ is the FW flux through a strait due to the mean FW concentration advected by the mean velocity, $v'_\perp \langle C_{FW} \rangle$ is the FW flux due to the advection of the mean FW concentration by the velocity anomaly, $C'_{FW} \langle v_\perp \rangle$ is the FW transport associated with the advection of FW concentration anomalies by the mean flow, and $C'_{FW} v'_\perp$ is the FW flux due to the advection of FW concentration anomalies by velocity anomalies. As $C'_{FW} v'_\perp$ is very small, it is not discussed in the following.

In Fram Strait, the FW export anomalies driven by FW concentration anomalies ($C'_{FW} \langle v_\perp \rangle$) and velocity anomalies ($v'_\perp \langle C_{FW} \rangle$) are of approximately equal importance for the variability of the total FW export (see Table 3 and Fig. 4a). In the CAA, velocity anomalies dominate the variability of the FW export, with a much smaller influence of FW concentration anomalies (see Table 3 and Fig. 4b). This agrees with model results of *Lique et al.* [2009], but not with model results of *Köberle and Gerdes* [2007] and *Jahn et al.* [2010a], who found no large influence of FW concentration changes on the variability of the Fram Strait FW export.

The different relative importance of FW concentration changes for the FW export variability through Fram Strait and the CAA explains why the FW export from all sources is largely in phase in the CAA, but not in phase in Fram Strait. In the next two subsections, we analyze the variability of the FW export from individual sources to further understand

the difference in the FW export variability between the two straits, and to see how FW from different sources contributes to the FW concentration changes.

4.2.1. Fram Strait

In Fram Strait, changes in the concentration of Eurasian runoff, Pacific FW, and NSIM explain a much larger percentage (>70%) of the variance of the FW export from each individual source than velocity changes (see Table 3 and Fig. 5a, c, d, g). This is surprising, given that (i) the Eurasian runoff and the Pacific FW are the two largest individual FW sources of the Fram Strait FW export, and (ii) the velocity and FW concentration anomalies contribute approximately equally to the variability of the total FW export in Fram Strait. However, the simulated FW concentration anomalies in Fram Strait from individual sources tend to partially balance each other (see Fig. 5), so that the total FW concentration anomaly in Fram Strait is reduced. Velocity changes, on the other hand, impact all FW sources at the same time, so that the resulting exports from distinct sources co-vary positively. This fundamental difference between FW export anomalies driven by velocity and by FW concentration anomalies is the reason why the concentration anomalies explain a much larger percentage of the variance of the FW export from individual FW sources than of the total FW export through Fram Strait.

Overall, the variability of the export of Pacific FW, of runoff from North America, from eastern Eurasia (Laptev and East Siberian seas), and from western Eurasia (Barents and Kara seas), of NSIM, and of net precipitation through Fram Strait is dominated by changes in the concentration of FW from these sources (see Table 3 and Fig. 5a, b, c, d, g, h). However, in contrast to NSIM and net precipitation, the variability of the export of FW from sea-ice melt, sea-ice formation, evaporation, and precipitation individually is

affected by both concentration and velocity anomalies (Table 3). Being able to separate NSIM and net precipitation into their individual contributions is therefore important.

4.2.2. CAA

As shown in Fig. 6a, b, e, f and Table 3, the largest part of the variance of the export of Pacific FW, North American runoff, sea-ice formation FW, and sea-ice melt FW through the CAA is explained by velocity anomalies. Concentration changes only dominate the variability of the FW export due to NSIM and Eurasian runoff (Fig. 6c, d, g and Table 3). For precipitation, evaporation and net precipitation, both FW concentration and velocity anomalies contribute to the export variability of FW through the CAA. Overall we find that concentration changes have a larger influence on the FW export variability of FW from individual sources than for the total CAA FW export, but velocity anomalies still dominate the variability of the FW export from all large individual FW sources. Furthermore, the sum of the concentration anomalies from Pacific FW, Eurasian runoff, North American runoff, and net precipitation nearly balance each other, due to an out-of-phase relationship between the concentration of Pacific FW and concentrations of FW from Eurasian runoff, North American runoff, and net precipitation. The total CAA export anomaly due to FW concentration changes is therefore small, and is almost identical to the NSIM concentration anomaly (r=0.88). We will analyze what is driving these FW concentration and velocity anomalies in section 5.2.

5. Atmospheric forcing mechanisms of the FW export variability

As shown in section 4, changes in the FW input do not directly cause the variability of the FW export, except for a small part of the Pacific FW export variability. Furthermore, it was shown that the variability of the CAA FW export is mainly controlled by velocity

anomalies, with only a small influence of FW concentration anomalies. In Fram Strait, on the other hand, velocity and FW concentration anomalies are equally important for the variability of the total FW export. In this section, we investigate the forcing mechanisms that cause the variability of the FW concentration and velocity in both straits. We find that the atmospheric forcing has a strong a impact on the liquid FW export variability, as shown, for example, by the spatial correlation pattern of the sea level pressure field (SLP) with the liquid FW export through Fram Strait (Fig. 7a) and the CAA (Fig. 7f). However, while the CAA FW export is mainly affected by large-scale atmospheric forcing resembling the Arctic Oscillation (AO) or the North Atlantic Oscillation (NAO), the Fram Strait FW export is affected mainly by the atmospheric forcing over the central Arctic Ocean (see Fig. 7a, f). This difference is due to the much larger influence of FW concentration anomalies on the variability of the FW in Fram Strait than in the CAA, because the FW concentration is mainly affected by SLP changed over the central Arctic (see Fig. 7c, h). The variability of the velocity in both straits, on the other hand, is mainly affected by the large-scale atmospheric circulation (see Fig. 7b, g). In the following, we will further investigate these forcing mechanisms and their effect on the variability of FW concentration and velocity in both straits.

5.1. Fram Strait

FW concentration anomalies in Fram Strait are largely caused by changes in the FW distribution upstream. Model results have shown that during phases of increased FW export through Fram Strait the concentration of FW along northern Greenland is increased [*Köberle and Gerdes*, 2007; *Condron et al.*, 2009; *Jahn et al.*, 2010a]. Using the FW tracers, we find that especially the Pacific FW concentration is strongly increased

north of Greenland during times when the Pacific FW concentration in Fram Strait is high (Fig. 8c). This simulated increase of Pacific water along the CAA and northern Greenland associated with an increased Pacific FW concentration in Fram Strait is in agreement with observational results of *Jones et al.* [2003] and *Newton and Sotirin* [1997]. To a lesser extend, Eurasian runoff (Fig. 8a–b), North American runoff (Fig. 8d), NSIM, and net precipitation (not shown) also show an increase in the FW storage north of Greenland when their concentration in Fram Strait is high. For Pacific FW, North American runoff, NSIM, and net precipitation, this is associated with a weaker Beaufort Gyre (Fig. 8c–d). This leads to a reduction of Ekman pumping, so that FW is released from the Beaufort Gyre [e.g., *Proshutinsky et al.*, 2002], which leads to the accumulation of FW previously stored in the Beaufort Gyre along the North American coast. The increase of the Eurasian runoff in Fram Strait and north of Greenland, on the other hand, is not associated with changes in the strength of the Beaufort Gyre, but with changes in the storage of Eurasian runoff on the shelves and changes in the path and strength of the TDS. This is not surprising, as the Eurasian runoff is mainly stored on the Eurasian shelves instead of the in Beaufort Gyre (see Fig. 8a–b). We find that the concentration of FW from eastern and western Eurasian runoff along northern Greenland is increased if the off-shelf transport of Eurasian runoff from the Laptev Sea is decreased (Fig. 8a). This is associated with a more cyclonic upper branch of the TDS (the part of the TDS directly adjacent to the Beaufort Gyre). At the same time, the lower branch of the TDS (the part of the TDS directly adjacent to the Barents Sea shelf break) is strengthened. The fundamental difference between the conditions under which Pacific and Eurasian FW distributions in the

Arctic Ocean change explains why the Fram Strait FW export from these two sources is not in phase.

As shown in Fig. 7d–e, the variability of Eurasian runoff and Pacific FW concentration anomalies in Fram Strait is linked to the variability of SLP over the central Arctic Ocean. However, the maximum correlation of the SLP field with the Eurasian runoff and Pacific FW concentrations in Fram Strait has opposite signs and occurs at different lags (Fig. 7d–e). This suggests that the above described changes in the FW distribution in the Arctic Ocean are best captured by an index that describes the atmospheric circulation in the central Arctic Ocean, rather than by larger-scale atmospheric indices like the AO or NAO index. We use here the Vorticity index, which describes shifts between cyclonic and anticyclonic circulation regimes in the Arctic [*Walsh et al.*, 1996], but the SLP at the North Pole gives similar results. Following *Dmitrenko et al.* [2008], the Vorticity index is calculated as the numerator of the finite difference Laplacian of the SLP in a radius of 500 km region around 85°N and 125°E (see green circle in Fig. 1). When the Vorticity index is positive, the atmospheric circulation in the central Arctic Ocean is cyclonic, with surface winds aligned with the Laptev Sea coast (see Fig. 9a). When the Vorticity index is negative, the atmospheric circulation in the central Arctic is anticyclonic, and the surface winds blow offshore in the western Laptev Sea (see Fig. 9b).

We find that the spatial pattern of the correlation between the Vorticity index and the FW storage in the Arctic Ocean has a dipole (see Fig. 10a), with positive correlations north of the CAA and Greenland and in most parts of the EGC, and with negative correlations in the western East Siberian and Laptev seas and in the region just north of the Eurasian shelf. This means that Eurasian runoff, especially from eastern Eurasia,

leaves the shelf during negative Vorticity index phases due to the offshore wind (Fig. 10b). Due to the cyclonic circulation anomaly over the central Arctic, Pacific FW, and to a lesser extent North American runoff, NSIM FW, and net precipitation FW, is released from the Beaufort Gyre during positive Vorticity index phases. Furthermore, while Eurasian runoff reaches Fram Strait with a 2–3 year delay after leaving the shelf (not shown), much of the FW released from the Beaufort Gyre reaches Fram Strait within 1 year. Consequently, the correlation of the Vorticity index and the total FW concentration anomaly in Fram Strait has a maximum positive correlation at a zero-to-one year lag due to the release of Pacific FW and other FW from the Beaufort Gyre during the positive Vorticity index phase. This is followed by a maximum negative correlation at a 3-year lag of the FW concentration anomaly behind the Vorticity index due to the reduced off-shelf transport of Eurasian runoff during positive Vorticity index phases (see Table 4 for the exact values of the correlation coefficients for all FW sources).

These simulation results for the relationship between the Vorticity index and the storage of FW on the Eurasian shelf are in agreement with a recent analysis of Russian hydrographic data on the Laptev and East Siberian shelves by *Dmitrenko et al.* [2008], who found the same relationship between FW storage on the Laptev and East Siberian Shelf and the Vorticity index. In fact, the cross-correlation plot between the Vorticity index and the FW storage shown in Fig. 10a matches the features shown in Fig. 9 of *Dmitrenko et al.* [2008], except for higher correlation coefficients of up to r=0.7 in *Dmitrenko et al.* [2008], compared to a maximum of r=0.4 found here. *Dmitrenko et al.* [2008] also used the summer Vorticity index and the summer FW storage, whereas Fig. 10a shows the annual Vorticity index and FW storage. If we use summer (JJAS) means, the same pattern

emerges in the eastern Arctic, but we miss the positive correlation between the Vorticity index and the FW storage along the coast of North America and Greenland and in the east Greenland current, which is the result of the winter Vorticity index (not shown).

The variance of the velocity-driven FW export is determined mainly (81%) by changes in the east-west SSH gradient across the EGC, which affects the geostrophic flow through Fram Strait. The variance of the SSH gradient in turn is found to be mainly (61%) controlled by changes in the SSH on the eastern edge of the EGC. The variability of the SSH on the eastern edge of the EGC is related to changes in the inflow from the Atlantic (r=−0.53) and changes in the salinity of the inflow (r=−0.43). This suggests that changes in the Atlantic inflow through Fram Strait can affect the geostrophic export from the Arctic through Fram Strait. This is in agreement with results from *Köberle and Gerdes* [2007], who found that a decrease in the salinity of the Atlantic inflow in the 1960s led to very low volume exports in the EGC during that time, due to changes in the steric height gradient across Fram Strait. The strength of the meridional wind in Fram Strait also influences the southward velocity in Fram Strait, as shown by a correlation of r=0.55 between the meridional wind and the velocity-driven FW export anomaly. The intensity of the meridional wind is in turn set by the east-west SLP gradient between Greenland and the western Barents Sea (r=0.98). Through changes in the SSH gradient across Fram Strait and in the meridional wind forcing, the large-scale atmospheric forcing affects the velocity driven FW export anomaly. Figure 7b shows that the SLP pattern correlated with the velocity anomalies of the FW export in Fram Strait is similar to the NAO pattern. However, the velocity anomaly in Fram Strait also has a correlation with the Vorticity index (see Table 4).

Due to the relationship between the Vorticity index and the FW concentration and velocity anomalies of the FW export in Fram Strait, the Vorticity index and the total liquid FW export through Fram Strait have a maximum correlation of r=0.37 at zero-year lag and r=−0.43 at a 3-year lag of the FW export behind the Vorticity index.

5.2. CAA

As shown in Fig. 7f–g, the CAA FW export as well as the velocity driven FW export anomaly in the CAA are affected by large-scale atmospheric forcing resembling the AO, in agreement with results of *Koenigk et al.* [2007] and *Jahn et al.* [2010a]. Consequently, the highest correlation between an atmospheric index and the CAA FW export is found for the AO index, with a maximum of r=0.47 for a zero-to-one year lag of the CAA FW export behind the AO index (for the 3-year running means). This correlation of the CAA FW export is entirely due to the link between the AO index and the velocity-driven CAA FW export anomaly (r=0.54 at zero-year lag). The AO index and the FW concentration-driven CAA FW export anomaly have no significant correlation.

The AO affects the variability of the ocean velocity in the CAA through its impact on the SSH gradient between the Beaufort Sea and Baffin Bay (r=0.46 at a 1-year lag of the SSH gradient) and on the along-strait wind forcing (r=0.58 at zero-year lag), as these two factors are found to drive the variability of the ocean velocity in the CAA. In our simulation, changes in the SSH gradient between the Beaufort Sea and northern Baffin Bay SSH explain 82% of the variance of the ocean velocity. This is in general agreement with observations [*Prinsenberg and Bennett*, 1987; *Kliem and Greenberg*, 2003] and previous model results [*Newton et al.*, 2008; *Jahn et al.*, 2010a]. The variability of the SSH gradient, in turn, is mainly influenced by changes of the SSH in Baffin Bay (r^2=0.70), with SSH

changes in the Beaufort Sea accounting for a smaller fraction of the variability (r^2=0.26). Extremely high or low simulated volume fluxes through the CAA are, however, always due to changes in the SSH in both regions (one example is the very low FW export in year 474 visible in Fig. 2b). Note that the SSH changes in the Beaufort Sea are mainly due to steric height changes associated with FW storage changes in the Beaufort Gyre (not shown). Consequently, FW storage anomalies in the Beaufort Gyre have some influence on the variability of the velocity in the CAA. In addition to the SSH gradient, the along-strait wind forcing in the CAA also explains 15% of the variance of the ocean velocity in the CAA. For the total FW export through the CAA, the SSH gradient can explain 84% of the variance and the along-strait wind forcing can explain 12%.

Beside the effect on the steric height in the Beaufort Sea, changes in the strength of the Beaufort Gyre also affect the FW concentration anomalies in the CAA. We find that during times when the Beaufort Gyre is weakened, the concentration of Pacific FW in the CAA is increased (Fig. 11a) because Pacific FW is released from the Beaufort Gyre due to weaker Ekman pumping. An increase in the concentration of FW from North American runoff in the CAA, on the other hand, is associated with a coastal cyclonic circulation anomaly in the Beaufort Sea, together with a stronger Beaufort Gyre (Fig. 11b). This causes the runoff to stay closer to the coast, instead of spreading out into the Beaufort Sea (Fig. 11b). The concentration of Eurasian runoff in the CAA is also increased during times when the Beaufort Gyre is stronger, because of more Eurasian runoff entrainment from the TDS (Fig. 11c, d). For the same reason, the concentration of FW from sea-ice melt and formation in the CAA is also increased during times of a stronger Beaufort Gyre (not shown). However, due to differences in the distribution of FW from sea-ice melt and

formation (the Eurasian shelf is an ice factory), the concentration of FW from sea-ice formation in the CAA increases more than FW from sea-ice melt. As NSIM is positive in the CAA at most times, this larger increase in FW from sea-ice formation than from melt leads to a smaller concentration of NSIM in the CAA during periods of a stronger Beaufort Gyre (not shown).

The difference between the conditions that cause increased concentrations of Pacific FW in the CAA compared to increased concentrations of FW from North American and Eurasian runoff explains the out-of-phase relationship between the Pacific FW concentration export anomaly and the FW export anomaly due to concentration changes of FW from runoff, which was mentioned in section 4.2. These FW concentration anomalies therefore cancel each other, and the total FW concentration anomaly in the CAA is roughly equal to the NSIM FW concentration anomaly (see section 4.2). Hence, a positive FW concentration anomaly exists in the CAA during times when the Beaufort Gyre is weak.

6. Discussion and Conclusion

Using a 140-year long 1990-equilibrium-simulation from the CCSM3 that includes FW tracers, we showed that the liquid FW export through Fram Strait is mainly due to Eurasian runoff (64%) and Pacific FW (48%), with smaller contributions from negative Atlantic FW (−18%), NSIM (−14%), North American runoff (9%), and net precipitation (5%). In the CAA, the liquid FW export mainly consists of Pacific FW (59%) and North American river runoff (32%), with smaller contributions from Eurasian runoff (7%), NSIM (7%), net-precipitation (3%), and negative Atlantic FW (−3%).

The interannual variability of the simulated Fram Strait FW export is driven by both changes in FW concentration and in velocity (which explain 36% and 43% of the variance, respectively). Due to a different mechanism behind the variability of the FW export from individual sources, the variability of the Fram Strait FW export shows no simple relationship with any large-scale atmospheric indices.

The largest correlation of the Fram Strait FW export with an atmospheric index is found for the Vorticity index (in a 550 km radius around 85°N and 125°E), which affects mainly the FW concentration in Fram Strait. For the total FW export through Fram Strait the correlation with the Vorticity index is r=0.37 at zero-year lag and r=−0.43 at a 3-year lag of the FW export behind the Vorticity index (for the 3-year running means). This two-peak correlation pattern is due to the two-fold effect of the atmospheric vorticity in the central Arctic Ocean on the different FW storage reservoirs: (i) Due to a release of Pacific FW from the Beaufort Gyre during years with a positive Vorticity index (cyclonic circulation anomaly), the Pacific FW concentration in Fram Strait increases within a year. (ii) The transport of river water off the Eurasian shelf is decreased during years with a positive Vorticity index [as also shown by *Dmitrenko et al.*, 2008, in observational data], which then affects the concentration of Eurasian runoff in Fram Strait about 3 years later.

The correlation of the Fram Strait FW export with the AO index is lower than with the Vorticity index, which shows that for the FW export through Fram Strait the local atmospheric conditions in the central Arctic Ocean are more important than the large-scale atmospheric circulation pattern. The southward velocity variability in Fram Strait, on the other hand, is driven largely by changes in Atlantic inflow, which affect the SSH on

the eastern edge of the ECG. These changes are related to large-scale atmospheric forcing resembling the NAO.

In the CAA, the velocity-driven FW export variability explains most (78%) of the variance of the simulated liquid FW export, with a smaller role of FW concentration changes (11%). Due to the dominant role of the velocity, the variability of the CAA liquid FW export is mainly driven by SSH changes between the Beaufort Sea and Baffin Bay (84%), with a smaller contribution from the along-strait wind (12%). As the SSH gradient and the along-strait wind are correlated with the AO index, the 3-year running mean of the total liquid CAA FW export also has a correlation of r=0.47 with the AO, at a 1-year lag of the FW export behind the AO index.

A higher cross-correlation with the AO index in the CAA compared to Fram Strait agrees with results of *Jahn et al.* [2010a] obtained from the University of Victoria Earth System Climate Model (UVic ESCM). However, *Jahn et al.* [2010a] found generally higher cross-correlations between the AO index and the FW export, and a lag of 2–6 years in Fram Strait, in contrast to what is found here. This difference might be partly due to the difference between model generated winds (CCSM3) and prescribed NCEP winds (UVic ESCM). More importantly, however, is the fact that changes in the FW concentration were found to be equally important for the variability of the Fram Strait FW export in the CCSM3 simulation, but were not important in the UVic ESCM simulation [*Jahn et al.*, 2010a]. We suggest that these differences in the importance of the FW concentration anomalies might be due in part to the lower vertical resolution of the UVic ESCM (top-layer-thickness of 50 m) compared to the 10 m top-layer-thickness in the CCSM3. A lower vertical resolution damps the variability of the salinity signal and hence changes the

simulated FW export variability. Support for the hypothesis that a high vertical resolution might indeed be important to resolve the role of FW concentration changes for the Fram Strait FW export variability comes from other model simulations with different vertical resolutions. *Köberle and Gerdes* [2007] used a model with a surface layer of 50 m, and found that FW concentration changes are not important for the variability of the Fram Strait export, similar to the UVic ESCM results. *Lique et al.* [2009], on the other hand, used a model with a surface layer thickness of 6 m, and found that FW concentration changes drive a large part of the variability in Fram Strait, similar to the CCSM3 results. We therefore suggest that a high vertical resolution is important for the proper simulation of the FW export variability in Fram Strait.

As the results presented here are from one model only, it would be desirable that other models also include FW tracers in the future, to test and refine the mechanisms proposed here. In addition, it is important to note that the channels between the New Siberian Islands (separating the East Siberian Sea and the Laptev Sea) and the Eurasian coast are closed in the CCSM3, due to the model resolution. As a result, the eastward transport of runoff from the Laptev Sea into the East Siberian Sea is small, and the simulated shifts in the shelf-basin exchange between the Lomonosov and Mendeleev ridge are not as large as described by *Schlosser et al.* [2002] and *Newton et al.* [2008]. Furthermore, the closed Nares Strait in the model affects the simulated partitioning between FW from different sources in Fram Strait as well as the magnitude of the FW export through Fram Strait and the CAA. In spite of these model shortcomings, the agreement between the simulated and observed features (e.g., the off-shelf transport of runoff during negative Vorticity index

phases and the contribution of FW from different sources to the FW export through the CAA and Fram Strait) gives credibility to the presented model results.

Climate simulations predict large changes in the Arctic during the 21st century, including a disappearance of the summer sea-ice cover [*Holland et al.*, 2006a; *Zhang and Walsh*, 2006; *Stroeve et al.*, 2008; *Wang and Overland*, 2009] and an increased liquid FW export from the Arctic [*Holland et al.*, 2006b, 2007; *Koenigk et al.*, 2007; *Arzel et al.*, 2008]. These changes might lead to changes in the Arctic Ocean circulation, as suggested by some model simulations. However, the direction of these changes remains unknown, due to contradicting model results. For instance, *Otterå and Drange* [2004] showed that under increased runoff and decreased sea-ice cover, the simulated Beaufort Gyre circulation is stronger due to increased horizontal density gradients in the central Arctic and a more efficient momentum transfer through the thinner sea-ice cover. However, *Gao et al.* [2009] found that in a $2 \times CO_2$ simulation, which has a similar climatic effect as prescribed by *Otterå and Drange* [2004], the TDS disappears and the Beaufort Gyre is much weaker. Even though these simulated changes in the circulation are very different, both would significantly change the FW pathways and export variability of FW from different sources. We next plan to investigate these future changes in the Arctic circulation in more detail, to study how the key mechanisms presented here might change during the 21st century.

Acknowledgments. We thank Keith Lindsay (NCAR) for help with the implementation of passive tracers into the CCSM3, and David Bailey (NCAR) for assistance with the set-up of the model and with NCL. Constructive comments from Rüdiger Gerdes (AWI), Jacques Derome (McGill University), and two anonymous reviewers helped us to improve the manuscript. This work was supported by grants from the "Studienstiftung

des deutschen Volkes", the Global Environmental and Climate Change Centre (GEC3), and Québec-Océan, awarded to Alexandra Jahn; two NSF Office of Polar Program Grants (OPP-0230325 and OPP-0230264), an NSERC Discovery Grant, and an Arctic Science Program Grant (ARC-0520496) awarded to B. Tremblay; and an NSERC Discovery Grant awarded to L. A. Mysak.

References

Aagaard, K., and E. C. Carmack (1989), The role of sea ice and other fresh water in the Arctic circulation, *J. Geophys. Res.*, *94*(C10), 14,485–14,498, doi: 10.1029/JC094iC10p14485.

Aagaard, K., J. H. Swift, and E. C. Carmack (1985), Thermohaline circulation in the Arctic Mediterranean seas, *J. Geophys. Res.*, *90*(C7), 4833–4846, doi: 10.1029/JC090iC03p04833.

AMAP (1998), *AMAP assessment report: Arctic pollution issues*, Arctic Monitoring and Assessment Programm (AMAP), Oslo, Norway, available at http://www.grida.no/amap.

Arzel, O., T. Fichefet, H. Goosse, and J.-L. Dufresne (2008), Causes and impacts of changes in the Arctic freshwater budget during the twentieth and twenty-first centuries in an AOGCM, *Clim. Dyn.*, *30*, 37–58, doi:10.1007/s00382-007-0258-5.

Bauch, D., P. Schlosser, and R. G. Fairbanks (1995a), Freshwater balance and the sources of deep and bottom waters in the Arctic Ocean inferred from the distribution of $H_2^{18}O$, *Prog. Oceanogr.*, *35*, 53–80.

Bauch, H. A., M. Kubisch-Popp, T. M. Cronin, and B. Rossak (1995b), A study of the calcareous microfauna from Laptev Sea sediments, in *Reports on Polar Research*, vol. 176, pp. 334–339, Alfred Wegener Institute for Polar and Marine Research, Bremerhaven.

Bitz, C. M., and W. H. Lipscomb (1999), An energy-conserving thermodynamic model of sea ice, *J. Geophys. Res.*, *104*(C7), 15,669–15,677, doi:10.1029/1999JC900100.

Björk, G., J. Söderkvist, P. Winsor, A. Nikolopoulos, and M. Steele (2002), Return of the cold halocline layer to the Amundsen Basin of the Arctic Ocean: Implications for the sea ice mass balance, *Geophys. Res. Lett.*, *29*(11), doi:10.1029/2001GL014157.

Briegleb, B. P., C. M. Bitz, E. C. Hunke, W. H. Lipscomb, M. M. Holland, J. L. Schramm, and R. E. Moritz (2004), Scientific description of the sea ice component of the Community Climate System Model, Version Three, *Tech. Rep. NCAR/TN-463+STR*, National Center for Atmospheric Research, Boulder, CO, 78 pp.

Collins, W. D., P. J. Rasch, B. A. Boville, J. J. Hack, J. R. McCaa, D. L. Williamson, J. T. Kiehl, B. Briegleb, C. Bitz, S.-J. Lin, M. Zhang, and Y. Dai (2004), Description of the NCAR Community Atmosphere Model (CAM 3.0), *Tech. Rep. NCAR/TN-464+STR*, National Center for Atmospheric Research, Boulder, CO, 226 pp.

Collins, W. D., C. M. Bitz, M. L. Blackmon, G. B. Bonan, C. S. Bretherton, J. A. Carton, P. Chang, S. C. Doney, J. J. Hack, T. B. Henderson, J. T. Kiehl, W. G. Large, D. S. McKenna, B. D. Santer, and R. D. Smith (2006a), The Community Climate System Model version 3 (CCSM3), *J. Climate*, *19*(11), 2122–2143, doi:10.1175/JCLI3761.1.

Collins, W. D., P. J. Rasch, B. A. Boville, J. J. Hack, J. R. McCaa, D. L. Williamson, B. P. Briegleb, C. M. Bitz, S.-J. Lin, and M. Zhang (2006b), The formulation and atmospheric simulation of the Community Atmosphere Model Version 3 (CAM3), *J.*

Climate, *19*(11), 2144–2161, doi:10.1175/JCLI3760.1.

Condron, A., P. Winsor, C. Hill, and D. Menemenlis (2009), Simulated response of the Arctic freshwater budget to extreme NAO wind forcing, *J. Climate*, *22*, 2422–2437, doi:10.1175/2008JCLI2626.1.

Dickinson, R. E., K. W. Oleson, G. Bonan, F. Hoffman, P. Thornton, M. Vertenstein, Z. L. Yang, and X. Zeng (2006), The Community Land Model and its climate statistics as a component of the Community Climate System Model, *J. Climate*, *19*(11), 2302–2324, doi:10.1175/JCLI3742.1.

Dmitrenko, I. A., S. A. Kirillov, and L. B. Tremblay (2008), The long-term and interannual variability of summer fresh water storage over the eastern Siberian shelf: Implications for climatic change, *J. Geophys. Res.*, *113*, doi:10.1029/2007JC004304.

Dodd, P. A., and E. Hansen (2009), The freshwater composition of the East Greenland Current derived from δ18O and N:P ratio measurements, *paper presented at MOCA-2009, IAMAS, IAPSO and IACS, Montreal, Canada*.

Dodd, P. A., K. J. Heywood, M. P. Meredith, A. C. Naveira-Garabato, A. D. Marca, and K. K. Falkner (2009), The sources and fate of freshwater exported in the East Greenland Current, *Geophys. Res. Lett.*, *36*, doi:10.1029/2009GL039663.

Falck, E., G. Kattner, and G. Budéus (2005), Disappearance of Pacific Water in northwestern Fram Strait, *Geophys. Res. Lett.*, *32*, doi:10.1029/2005GL023400.

Gao, Y., H. Drange, O. M. Johannessen, and L. H. Pettersson (2009), Sources and pathways of 90Sr in the North Atlantic-Arctic region: present day and global warming, *J. Environ. Radioact.*, *100*(5), 375–395, doi:10.1016/j.jenvrad.2009.01.003.

Gent, P. R., and J. C. McWilliams (1990), Isopycnal mixing in ocean circulation models, *J. Phys. Oceanogr.*, *20*(1), 150–155, doi:10.1175/1520-0485(1990)020<0150:IMIOCM>2.0.CO;2.

Gerdes, R., J. Hurka, M. Karcher, F. Kauker, and C. Koeberle (2005), Simulated history of convection in the Greenland and Labrador seas 1948–2001, in *The Nordic Seas: An Integrated Perspective*, *AGU, Geophysical Monograph*, vol. 158, edited by H. Drange, T. Dokken, T. Furevik, R. Gerdes, and W. Berger, pp. 221–238.

Häkkinen, S. (1995), Simulated interannual variability of the Greenland Sea Deep Water formation and its connection to surface forcing, *J. Geophys. Res.*, *100*(C3), 4761–4770, doi:10.1029/94JC01900.

Häkkinen, S., and A. Proshutinsky (2004), Freshwater content variability in the Arctic Ocean, *J. Geophys. Res.*, *109*, doi:10.1029/2003JC001940.

Harms, I. H., M. J. Karcher, and D. Dethleff (2000), Modelling Siberian river runoff - implications for contaminant transport in the Arctic Ocean, *J. Mar. Syst.*, *27*, 95–115, doi:10.1016/S0924-7963(00)00062-2.

Holland, M. M., C. M. Bitz, M. Eby, and A. J. Weaver (2001), The role of ice-ocean interactions in the variability of the North Atlantic thermohaline circulation, *J. Climate*, *14*(5), 656–675, doi:10.1175/1520-0442(2001)014<0656:TROIOI>2.0.CO;2.

Holland, M. M., C. M. Bitz, and B. Tremblay (2006a), Future abrupt reductions in the summer Arctic sea ice, *Geophys. Res. Lett.*, *33*, doi:10.1029/2006GL028024.

Holland, M. M., J. Finnis, and M. C. Serreze (2006b), Simulated Arctic Ocean freshwater budgets in the twentieth and twenty-first centuries, *J. Climate*, *19*(23), 6221–6242, doi:10.1175/JCLI3967.1.

Holland, M. M., J. Finnis, A. P. Barrett, and M. C. Serreze (2007), Projected changes in Arctic Ocean freshwater budgets, *J. Geophys. Res.*, *112*, doi:10.1029/2006JG000354.

Hunke, E. C., and J. K. Dukowicz (1997), An elastic-viscous-plastic model for sea ice dynamics, *J. Phys. Oceanogr.*, *27*(9), 1849–1867, doi:10.1175/1520-0485(1997)027<1849:AEVPMF>2.0.CO;2.

Hunkins, K., and J. A. Whitehead (1992), Laboratory simulation of exchange through Fram Strait, *J. Geophys. Res.*, *97*(C7), 11,299–11,321, doi:10.1029/92JC00735.

IPCC (2007), Climate Change 2007 - The Physical Science Basis. Contribution of Working Group I to the Fourth Assessment Report of the IPCC, in *IPCC Fourth Assessment Report "Climate Change 2007"*, edited by S. Solomon, D. Qin, M. Manning, Z. Chen, M. Marquis, K. Averyt, M. Tignor, and H. Miller, Cambridge University Press, Cambridge, United Kingdom and New York, NY, USA, 996 pp.

Jahn, A., B. Tremblay, L. A. Mysak, and R. Newton (2010a), Effect of the large-scale atmospheric circulation on the Arctic Ocean freshwater and heat exchange, *Clim. Dyn.*, *34*(2–3), 201–222, doi:10.1007/s00382-009-0558-z.

Jahn, A., L. B. Tremblay, R. Newton, M. M. Holland, and L. A. Mysak (2010b), Seasonal cycle of the Fram Strait freshwater export: A model perspective, *paper presented at State of the Arctic, Arctic Research Consortium of the U.S., Miami, USA*.

Jones, E. P., J. H. Swift, L. G. Anderson, M. Lipizer, G. Civitarese, and K. K. Falkner (2003), Tracing Pacific water in the North Atlantic Ocean, *J. Geophys. Res.*, *108*(C4), doi:10.1029/2001JC001141.

Jones, E. P., L. G. Anderson, S. Jutterström, and J. H. Swift (2008), Sources and distribution of fresh water in the East Greenland Current, *Prog. Oceanogr.*, *78*, 37–44,

doi:10.1016/j.pocean.2007.06.003.

Karcher, M., R. Gerdes, F. Kauker, C. Köberle, and I. Yashayaev (2005), Arctic Ocean change heralds North Atlantic freshening, *Geophys. Res. Lett.*, *32*, doi: 10.1029/2005GL023861.

Karcher, M. J., and J. M. Oberhuber (2002), Pathways and modification of the upper and intermediate waters of the Arctic Ocean, *J. Geophys. Res.*, *107*(C6), doi: 10.1029/2000JC000530.

Kliem, N., and D. A. Greenberg (2003), Diagnostic simulations of the summer circulation in the Canadian Arctic Archipelago, *Atmos.-Ocean*, *41*(4), 273–289.

Köberle, C., and R. Gerdes (2007), Simulated variability of the Arctic Ocean freshwater balance 1948–2001, *J. Phys. Oceanogr.*, *37*(6), 1628–1644, doi:10.1175/JPO3063.1.

Koenigk, T., U. Mikolajewicz, H. Haak, and J. Jungclaus (2007), Arctic freshwater export in the 20th and 21st centuries, *J. Geophys. Res.*, *112*, doi:10.1029/2006JG000274.

Large, W. G., J. C. McWilliams, and S. C. Doney (1994), Oceanic vertical mixing: A review and a model with a nonlocal boundary layer parameterization, *Rev. Geophys.*, *32*(4), 363–403, doi:10.1029/94RG01872.

Lique, C., A. M. Treguier, M. Scheinert, and T. Penduff (2009), A model based study of ice and freshwater transport variability along both sides of Greenland, *Clim. Dyn.*, *33*(5), 685–705, doi:10.1007/s00382-008-0510-7.

Lohmann, G., and R. Gerdes (1998), Sea ice effects on the sensitivity of the thermohaline circulation, *J. Climate*, *11*(11), 2789–2803, doi:10.1175/1520-0442(1998)011<2789:SIEOTS>2.0.CO;2.

Macdonald, R. W., D. Mackay, Y.-F. Li, and B. Hickie (2003), How will global climate change affect risks from long-range transport of persistent organic pollutants?, *Hum. Ecol. Risk. Assess.*, *9*(3), 643–660, doi:10.1080/713609959.

Macdonald, R. W., T. Harner, and J. Fyfe (2005), Recent climate change in the Arctic and its impact on contaminant pathways and interpretation of temporal trend data, *Sci. Total Environ.*, *342*, 5–86, doi:10.1016/j.scitotenv.2004.12.059.

Martinson, D. G., and M. Steele (2001), Future of the Arctic sea ice cover: Implications of an Antarctic analog, *Geophys. Res. Lett.*, *28*(2), 307–310, doi:10.1029/2000GL011549.

Maslowski, W., B. Newton, P. Schlosser, A. Semtner, and D. Martinson (2000), Modeling recent climate variability in the Arctic Ocean, *Geophys. Res. Lett.*, *27*(22), 3743–3746, doi:10.1029/1999GL011227.

Meredith, M., K. Heywood, P. Dennis, L. Goldson, R. White, E. Fahrbach, U. Schauer, and S. Østerhus (2001), Freshwater fluxes through the western Fram Strait, *Geophys. Res. Lett.*, *28*(8), 1615–1618, doi:10.1029/2000GL011992.

Münchow, A., H. Melling, and K. K. Falkner (2006), An observational estimate of volume and freshwater flux leaving the Arctic Ocean through Nares Strait, *J. Phys. Oceanog.*, *36*(11), 2025–2041, doi:10.1175/JPO2962.1.

Myers, P. G. (2005), Impact of freshwater from the Canadian Arctic Archipelago on Labrador Sea Water formation, *Geophys. Res. Lett.*, *32*, doi:10.1029/2004GL022082.

Nazarenko, L., G. Holloway, and N. Tausnev (1998), Dynamics of transport of "Atlantic signature" in the Arctic Ocean, *J. Geophys. Res.*, *103*(C13), 31,003–31,015, doi:10.1029/1998JC900017.

Newton, B., L. B. Tremblay, M. A. Cane, and P. Schlosser (2006), A simple model of the Arctic Ocean response to annular atmospheric modes, *J. Geophys. Res.*, *111*, doi: 10.1029/2004JC002622.

Newton, J. L., and B. J. Sotirin (1997), Boundary undercurrent and water mass changes in the Lincoln Sea, *J. Geophys. Res*, *102*(C2), 3393–3403, doi:10.1029/96JC03441.

Newton, R., P. Schlosser, D. Martinson, and W. Maslowski (2008), Freshwater distribution in the Arctic Ocean: simulation with a high-resolution model and model-data comparison, *J. Geophys. Res.*, *113*, doi:10.1029/2007JC004111.

Nilsson, J., G. Björk, B. Rudels, P. Winsor, and D. Torres (2008), Liquid freshwater transport and polar surface water characteristics in the East Greenland Current during the AO-02 Oden expedition, *Prog. Oceanog.*, *78*(1), 45–57, doi: 10.1016/j.pocean.2007.06.002.

Oleson, K. W., Y. Dai, G. Bonan, M. Bosilovich, R. Dickinson, P. Dirmeyer, F. Hoffman, P. Houser, S. Levis, G.-Y. Niu, P. Thornton, M. Vertenstein, Z.-L. Yang, and X. Zeng (2004), Technical description of the Community Land Model (CLM, *Tech. Rep. NCAR/TN-461+STR*, National Center for Atmospheric Research, Boulder, CO, 174 pp.

Östlund, H. G., and G. Hut (1984), Arctic Ocean water mass balance from isotope data, *J. Geophys. Res*, *89*(C4), 6373–638, doi:10.1029/JC089iC04p06373.

Otterå, O. H., and H. Drange (2004), A possible coupling between Arctic fresh water, the Arctic sea ice cover and the North Atlantic Drift. A case study, *Adv. Atm. Sci.*, *21*(5), 784–801.

Prange, M., and R. Gerdes (2006), The role of surface freshwater flux boundary conditions in Arctic Ocean modelling, *Ocean Model.*, *13*(1), 25–43, doi: 10.1016/j.ocemod.2005.09.003.

Prinsenberg, S. J., and E. B. Bennett (1987), Mixing and transport in Barrow Strait, the central part of the Northwest Passage, *Cont. Shelf Res.*, *7*(8), 913–935, doi: 10.1016/0278-4343(87)90006-9.

Proshutinsky, A., R. H. Bourke, and F. A. McLaughlin (2002), The role of the Beaufort Gyre in Arctic climate variability: Seasonal to decadal climate scales, *Geophys. Res. Lett.*, *29*(23), doi:10.1029/2002GL015847.

Proshutinsky, A., R. Krishfield, M.-L. Timmermans, J. Toole, E. Carmack, F. McLaughlin, W. J. Williams, S. Zimmermann, M. Itoh, and K. Shimada (2009), Beaufort Gyre freshwater reservoir: State and variability from observations, *J. Geophys. Res.*, *114*, doi:10.1029/2008JC005104.

Rabe, B., U. Schauer, A. Mackensen, M. Karcher, E. Hansen, and A. Beszczynska-Möller (2009), Freshwater components and transports in the Fram Strait - recent observations and changes since the late 1990s, *Ocean Science*, *5*(3), 219–233.

Rennermalm, A. K., E. F. Wood, S. J. Déry, A. J. Weaver, and M. Eby (2006), Sensitivity of the thermohaline circulation to Arctic Ocean runoff, *Geophys. Res. Lett.*, *33*, doi: 10.1029/2006GL026124.

Rennermalm, A. K., E. F. Wood, A. J. Weaver, M. Eby, and S. J. Déry (2007), Relative sensitivity of the Atlantic Meridional Overturning Circulation to river discharge into Hudson Bay and the Arctic Ocean, *J. Geophys. Res.*, *112*, doi:10.1029/2006JG000330.

Rutgers van der Loeff, M. M., R. M. Key, J. Scholten, D. Bauch, and A. Michael (1995), ^{228}Ra as a tracer for shelf water in the Arctic Ocean, *Deep-Sea Res.*, *42*(6), 1533–1553.

Schlosser, P., D. Bauch, R. Fairbanks, and G. Bönisch (1994), Arctic river runoff: mean residence time on the shelves and in the halocline, *Deep-Sea Research 1*, *41*, 1053–1068, doi:10.1016/0967-0637(94)90018-3.

Schlosser, P., B. Newton, B. Ekwurzel, S. Khatiwala, R. Mortlock, and R. Fairbanks (2002), Decrease of river runoff in the upper waters of the Eurasian Basin, Arctic Ocean, between 1991 and 1996: Evidence from δ^{18}O data, *Geophys. Res. Lett.*, *29*(9), doi:10.1029/2001GL013135.

Serreze, M. C., A. P. Barrett, A. G. Slater, R. A. Woodgate, K. Aagaard, R. B. Lammers, M. Steele, R. Moritz, M. Meredith, and C. M. Lee (2006), The large-scale freshwater cycle of the Arctic, *J. Geophys. Res.*, *111*, doi:10.1029/2005JC003424.

Smith, R., and P. Gent (2004), Reference manual for the Parallel Ocean Program (POP): Ocean component of the Community Climate System Model (CCSM2.0 and 3.0), *Tech. Rep. LAUR-02-2484*, Los Alamos National Laboratory, Los Alamos, NM, 75 pp.

Steele, M., and T. Boyd (1998), Retreat of the cold halocline layer in the Arctic Ocean, *J. Geophys. Res.*, *103*(C5), 10,419–10,435.

Stroeve, J., M. Serreze, S. Drobot, S. Gearheard, M. Holland, J. Maslanik, W. Meier, and T. Scambos (2008), Arctic sea ice extent plummets in 2007, *Eos Trans. AGU*, *89*(2), 13–14, doi:10.1029/2008EO020001.

Taylor, J. R., K. Falkner, U. Schauer, and M. Meredith (2003), Quantitative considerations of dissolved barium as a tracer in the Arctic Ocean, *J. Geophys. Res.*, *108*(C12), doi:10.1029/2002JC001635.

Thorndike, A. S., D. S. Rothrock, G. A. Maykut, and R. Colony (1975), Thickness distribution of sea ice, *J. Geophys. Res.*, *80*(C33), 4501–4513, doi:10.1029/JC080i033p04501.

Walsh, J. E., W. L. Chapman, and T. L. Shy (1996), Recent decrease of sea level pressure in the central Arctic, *J. Climate*, *9*(2), 480–486, doi:10.1175/1520-0442(1996)009<0480:RDOSLP>2.0.CO;2.

Wang, M., and J. E. Overland (2009), A sea ice free summer Arctic within 30 years?, *Geophys. Res. Lett.*, *36*, doi:10.1029/2009GL037820.

Weatherly, J. W., and J. E. Walsh (1996), The effects of precipitation and river runoff in a coupled ice-ocean model of the Arctic, *Clim. Dyn.*, *12*, 785–798, doi:10.1007/s003820050143.

Weaver, A. J., J. Marotzke, P. F. Cummins, and E. Sarachik (1993), Stability and variability of the thermohaline circulation, *J. Phys. Oceanogr.*, *23*(1), 39–60, doi:10.1175/1520-0485(1993)023<0039:SAVOTT>2.0.CO;2.

Woodgate, R. A., and K. Aagaard (2005), Revising the Bering Strait freshwater flux into the Arctic Ocean, *Geophys. Res. Lett.*, *32*, doi:10.1029/2004GL021747.

Yamamoto-Kawai, M., F. A. McLaughlin, E. C. Carmack, S. Nishino, and K. Shimada (2008), Freshwater budget of the Canada Basin, Arctic Ocean, from salinity, δ^{18}O, and nutrients, *J. Geophys. Res.*, *113*, doi:10.1029/2006JC003858.

Zhang, X., and J. E. Walsh (2006), Toward a seasonally ice-covered Arctic Ocean: Scenarios from the IPCC AR4 model simulations, *J. Climate*, *19*, 1730–1747, doi:10.1175/JCLI3767.1.

Zhang, X., M. Ikeda, and J. Walsh (2003), Arctic sea ice and freshwater changes driven by the atmospheric leading mode in a coupled sea ice-ocean model, *J. Climate*, *16*(13),

2159–2177, doi:10.1175/2758.1.

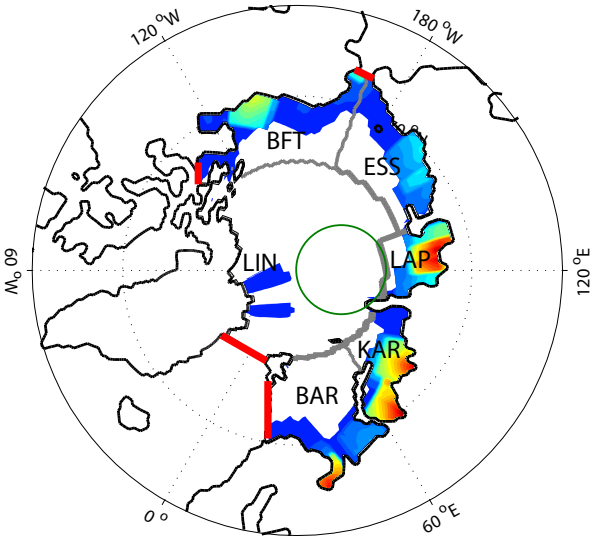

Figure 1. Map showing the land/ocean configuration of the CCSM3 (black outline) and the ocean boundaries used to calculate oceanic FW fluxes (red lines). Note that the CAA consists only of Barrow Strait in this model, as Nares Strait is closed. As explained in the text, the surface flux due to river runoff, and hence also the runoff tracer, is spread out into the ocean (see shaded colors), with highest concentrations (warm shaded colors) added at the coasts. The boundaries (grey lines) and names of the shelf basins used to add the tracer for runoff into the Beaufort Sea (BFT), East Siberian Sea (ESS), Laptev Sea (LAP), Kara Sea (KAR), Barents Sea (BAR), and Lincoln Sea (LIN) are also shown. The area used to calculate the Vorticity index used in section 5 is outlined in green.

Table 1. Climatological Arctic Ocean freshwater (FW) budget based on the CCSM3 1990 equilibrium simulation (averaged over simulation years 440–539) and on observations. In the first column, the FW fluxes calculated relative to 34.7 are shown. 34.7 is the reference salinity used to calculate the virtual salt fluxes in the CCSM3, and the reference salinity used in the rest of the article. For comparison with observations and other studies, column two shows the CCSM3 fluxes relative to 34.8. Column three shows the observational FW budget, relative to a reference salinity of 34.8. All observational values are taken from *Serreze et al.* [2006], except for the Bering Strait sea-ice flux, which is based on *Woodgate and Aagaard* [2005]. All FW fluxes are given in km^3/year. They are net annual mean fluxes through a channel, combining negative and positive fluxes through a strait, where applicable. All oceanic fluxes are calculated over the full depth of the water column at the boundaries. Positive values indicate FW sources, and negative values indicate FW sinks for the Arctic Ocean. Note that because Nares Strait is closed in the model, the Fram Strait FW fluxes include FW fluxes that should go through Nares Strait.

FW fluxes	CCSM3 S_{Ref}=34.7	CCSM3 S_{Ref}=34.8	Observations S_{Ref}=34.8
River runoff	4281	4281	3200
Net precipitation	2002	2002	2000
Bering Strait solid FW	124	124	100
CAA solid FW	−52	−52	−160
Fram Strait solid FW	−2238	−2239	−2300
Barents Sea Opening solid FW	−9	−9	–
Bering Strait liquid FW	3033	3111	2500
CAA liquid FW	−1569	−1598	−3200
Fram Strait liquid FW	−4929	−5405	−2660
Barents Sea Opening liquid FW	−1218	−786	−90
Net	−575	−571	−610

Table 2. Contribution of FW from different sources (calculated from the tracers) to the total liquid FW export (calculated from the salinity) from the Arctic Ocean. The first number gives the amount in km^3/yr, followed by the percentage of how much FW from an individual source contributes to the total liquid FW export (calculated from salinities) through each strait. In difference to Table 1, which showed the net fluxes over the full depth, this table shows southward fluxes in the top 247 m only. Negative numbers stand for an export of negative FW. "Rest" stands for the part of the liquid FW export that is not accounted for by the FW tracers, for reasons explained in section 3.1.

Source of FW	Fram Strait		CAA	
Barents Sea runoff	603	10.4%	11	0.7%
Kara Sea runoff	1595	27.6%	19	1.2%
Laptev Sea runoff	1070	18.3%	43	2.8%
East Siberian Sea runoff	452	7.7%	35	2.2%
Beaufort Sea runoff	266	4.6%	480	30.4%
Lincoln Sea runoff	249	4.3%	20	1.3%
Precipitation	1230	21.3%	109	7.0%
Evaporation	−925	−16.0%	−68	−4.3%
Sea-ice melt	8881	153.0%	1910	122.0%
Sea-ice formation	−9676	−166.9%	−1795	−114.9%
Pacific FW	2788	47.9%	930	59.1%
Atlantic FW	−1028	−17.8%	−43	−2.8%
Rest	325	5.6%	−74	−4.7%
Total FW	5830	100%	1577	100%

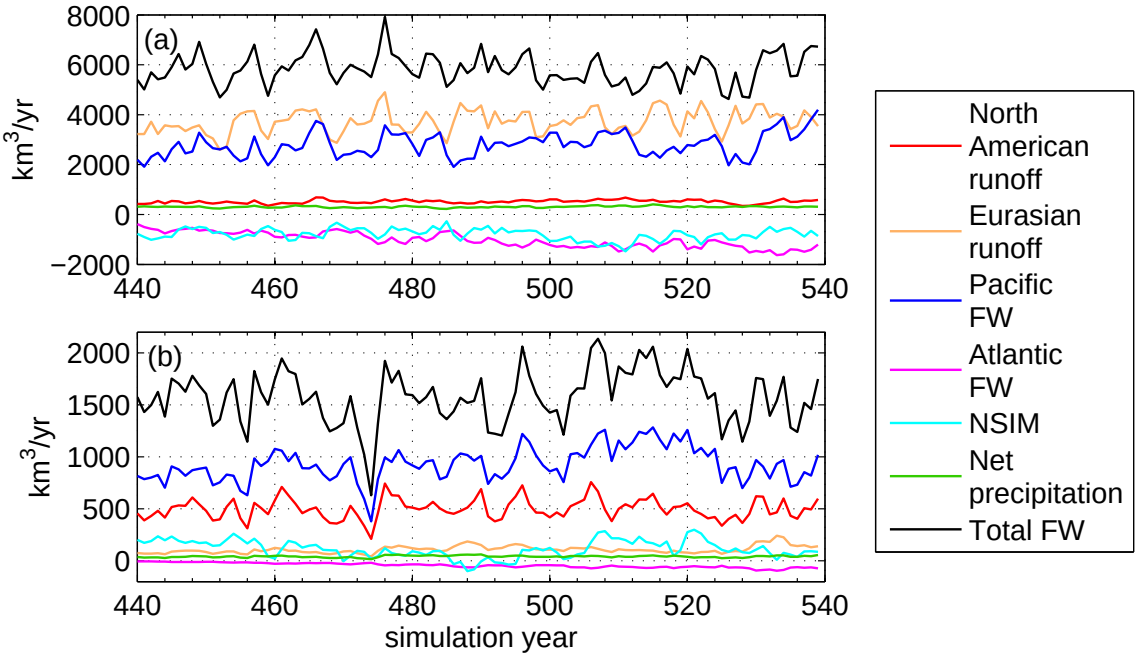

Figure 2. Total liquid FW (calculated from salinity) and FW tracer exports [km^3/yr] through (a) Fram Strait (top 247 m, outflow only) and (b) the CAA. Positive fluxes stand for an export of FW, negative fluxes for an export of negative FW. The average simulated FW fluxes due to FW from each tagged source are listed in Table 2.

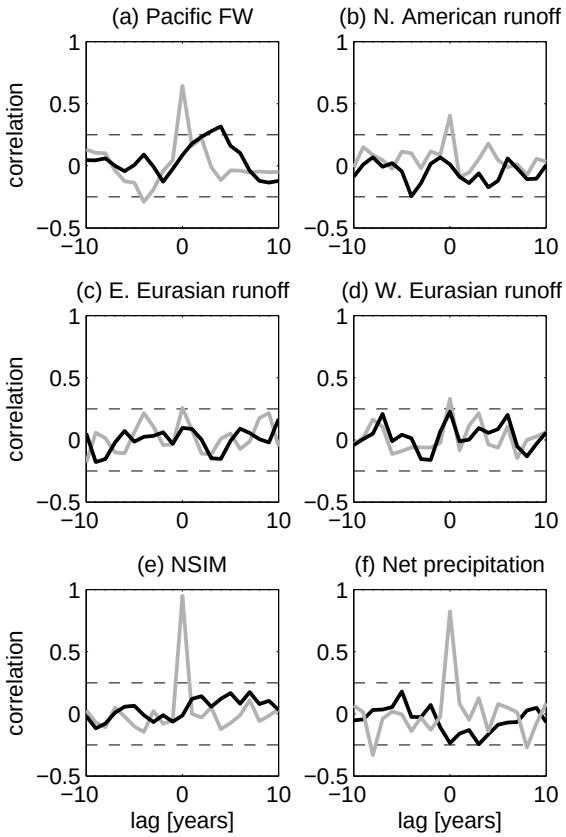

Figure 3. Cross-correlation between the annual FW input and the total annual export of liquid FW (through Fram Strait, CAA, and the Barents Sea Opening combined) from different sources (black lines in a–f). This shows how much the input variability from each source affects the variability of the FW export. Also shown is the cross-correlation between the annual FW inputs from different sources and the time derivative of the storage of FW from these sources in the Arctic Ocean (grey lines in a–f), which shows how much changes in the FW input affect the FW storage. The 95% significance level for all correlations is indicated by dashed black lines. A positive lag means that the FW input leads the FW export.

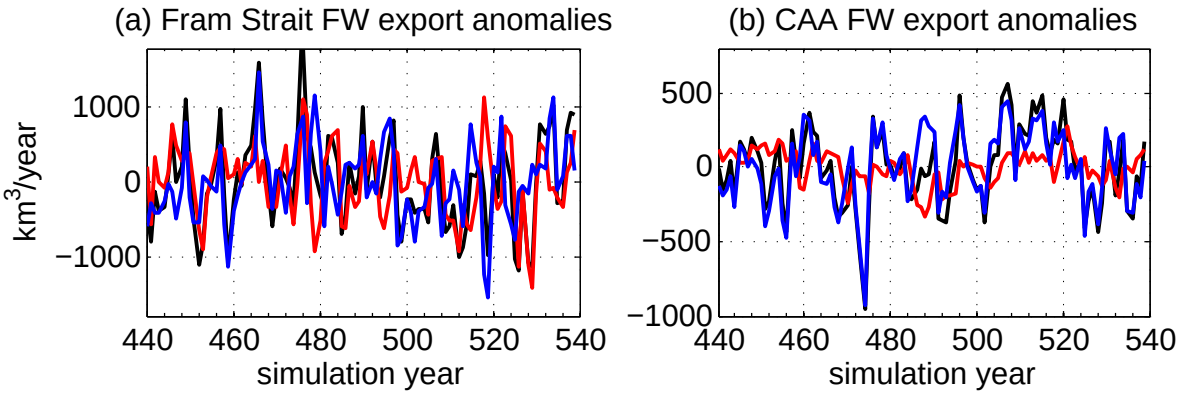

Figure 4. FW export anomaly for (a) Fram Strait and (b) CAA, split up into contributions from FW concentration changes ($C'_{FW}\,\langle v_\perp \rangle$, in red) and from velocity changes ($v'_\perp\,\langle C_{FW} \rangle$, in blue). FW export anomalies from the advection of FW concentration anomalies by the velocity anomaly ($C'_{FW}\,v'_\perp$) are very small, and not shown. The total liquid FW export anomaly due to FW from each source is shown as black line. Positive values show an increased FW export compared to the mean, and negative values a decreased FW export.

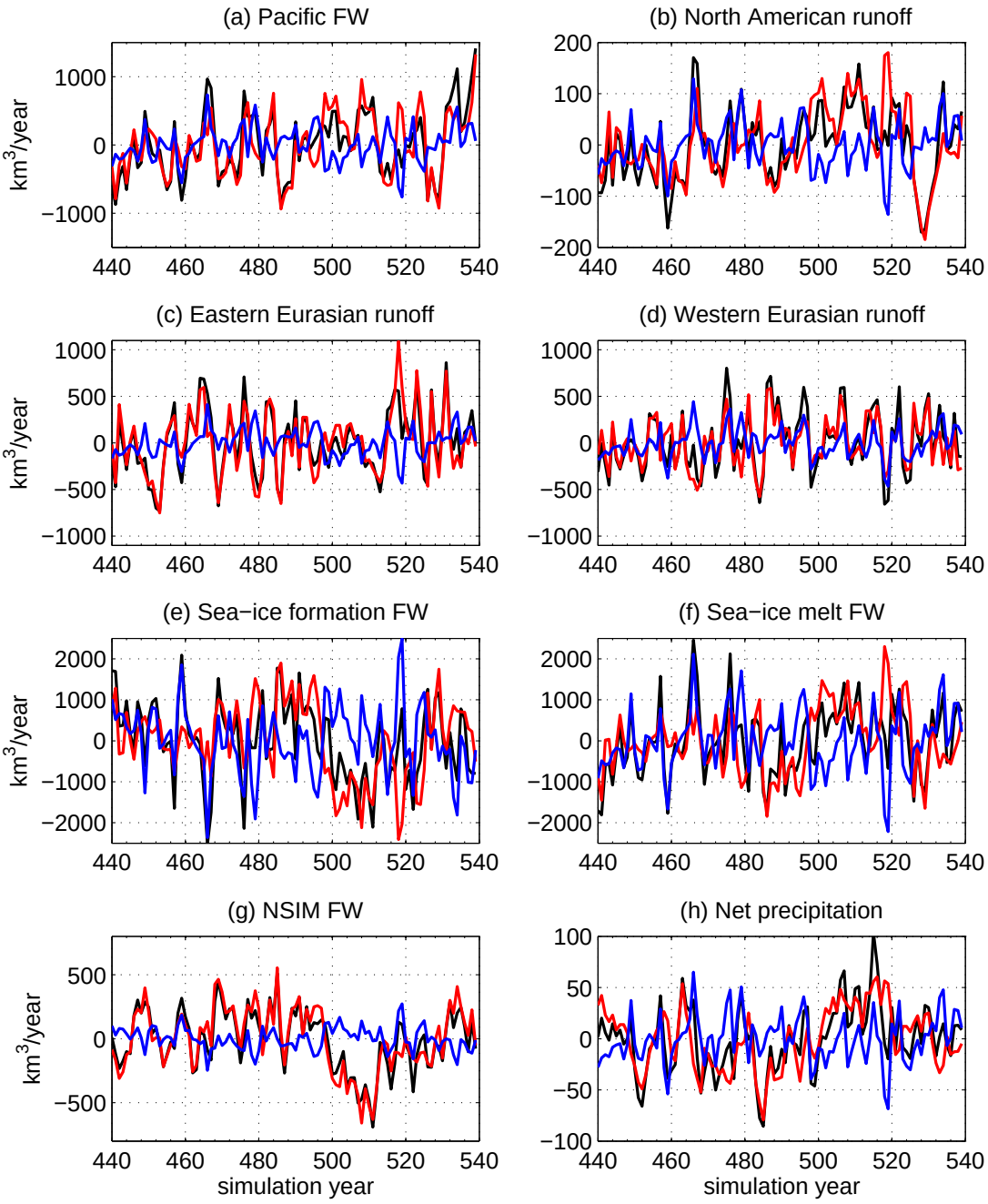

Figure 5. As Fig. 4a, but split up into FW from different sources, to show whether FW concentration or velocity anomalies dominate the export variability of FW from different sources. In red, FW export anomalies due to FW concentration changes ($C'_{FW}\,\langle v_\perp \rangle$), and in blue FW export anomalies due to velocity anomalies ($v'_\perp\,\langle C_{FW} \rangle$). FW export anomalies from the advection of FW concentration anomalies by the velocity anomaly ($C'_{FW}\,v'_\perp$) are very small, and not shown. The total liquid FW export anomaly due to FW from each source is shown as black line. Note the different scales in the different panels. Also note that because the NSIM and ice formation export is negative in Fram Strait, a negative anomaly in (e) and (g) indicates an increased export of negative FW.

Table 3. The variance (r^2 values) of the total FW export and the FW export from individual sources that is explained by FW concentration anomalies ($C'_{FW}\,\langle v_\perp \rangle$) and velocity anomalies ($v'_\perp\,\langle C_{FW} \rangle$). This indicates whether the export variability in Fram Strait and the CAA is mainly due to changes in the concentration of FW, or whether it is due to changes in the amount of water leaving the Arctic. All listed r^2 values are statistically significant at the 95% confidence level.

Source of FW	Fram Strait		CAA	
	$C'_{FW}\,\langle v_\perp \rangle$	$v'_\perp\,\langle C_{FW} \rangle$	$C'_{FW}\,\langle v_\perp \rangle$	$v'_\perp\,\langle C_{FW} \rangle$
Total FW export	0.36	0.43	0.11	0.78
Pacific FW	0.70	0.14	0.25	0.78
North American runoff	0.57	0.14	0.33	0.70
Eastern Eurasian runoff	0.82	0.05	0.78	0.31
Western Eurasian runoff	0.76	0.30	0.86	0.26
Sea-ice formation	0.36	0.22	0.38	0.68
Sea-ice melt	0.33	0.28	0.18	0.79
NSIM	0.86	not sign.	0.92	not sign.
Precipitation	0.32	0.56	0.57	0.60
Evaporation	0.41	0.59	0.60	0.58
Net precipitation	0.53	0.18	0.56	0.58

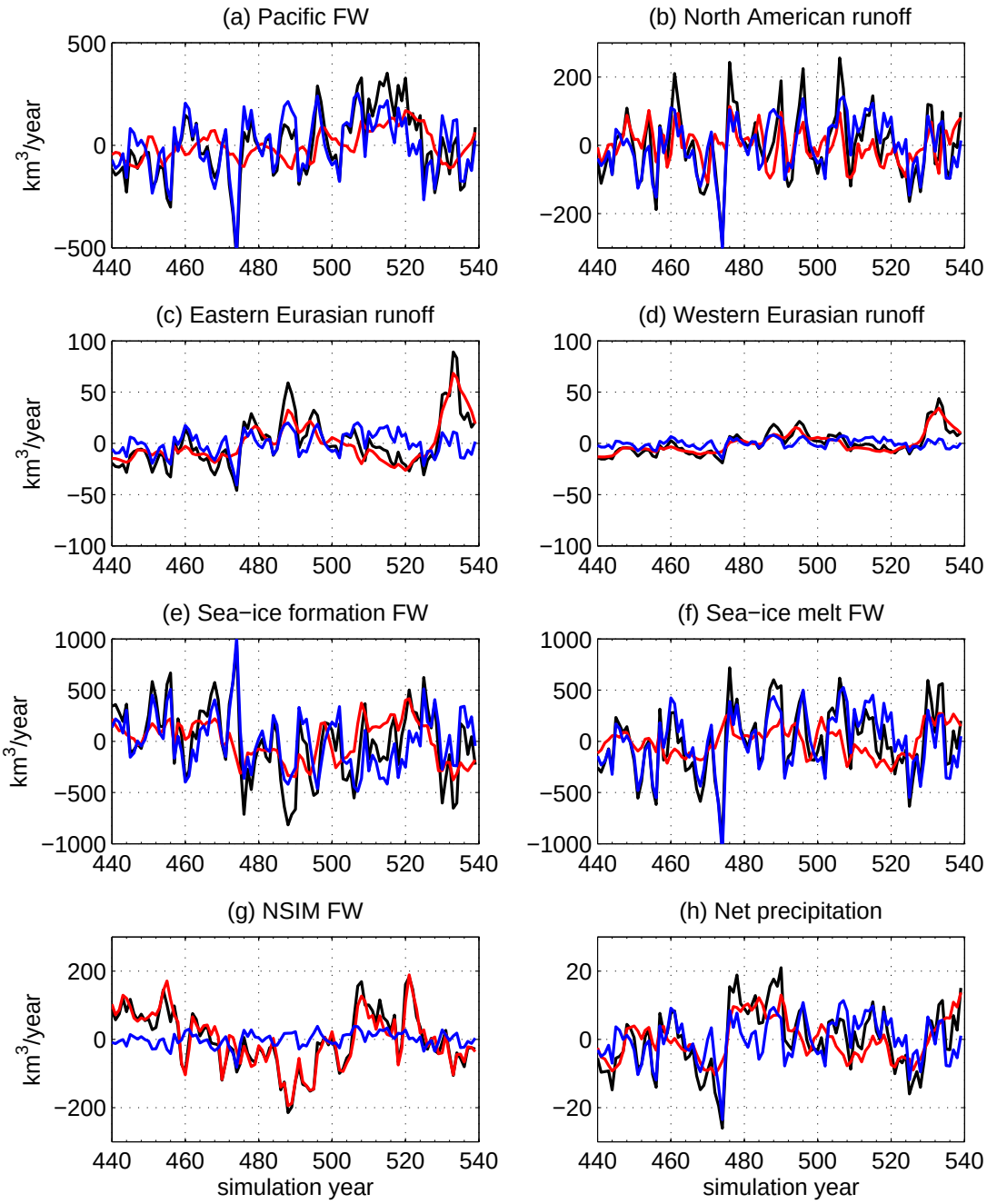

Figure 6. As Fig. 5, but for the CAA FW export. Note that the CAA export due to NSIM is on average positive (i.e. more sea-ice melt than sea-ice formation), except between simulation years 486–495. This means that negative anomalies of NSIM indicate a smaller export of positive NSIM, except between 486–495, when negative anomalies indicate an increased export of negative NSIM.

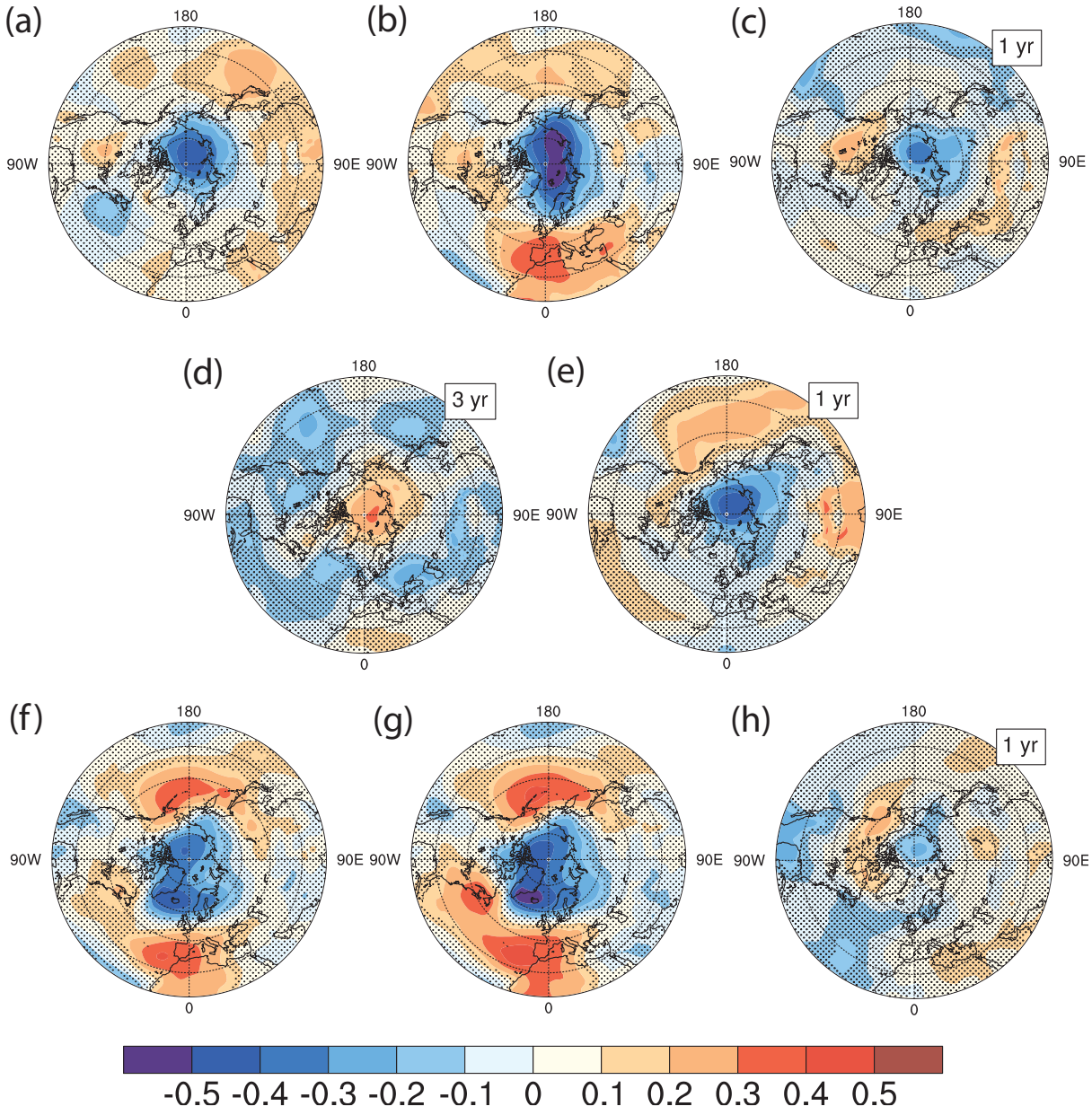

Figure 7. In the top row (a–c), correlations between the SLP field and the total FW export (a), the velocity driven FW export anomaly (b), and the FW concentration driven FW export anomaly (c) for Fram Strait are shown. In the middle row (d–e), the correlation between the SLP field and the Eurasian runoff (d) and Pacific FW (e) concentration anomalies in Fram Strait is shown. In the bottom row (f–h), the correlation between the SLP field and the total FW export (f), the velocity driven FW export anomaly (g), and the FW concentration driven FW export anomaly (h) for the CAA are shown. Correlation fields are shown for the year with the maximum correlation, and the lag (if $>$ 0 years) is given in the top right corner (in years). Correlations not significant at the 95% level are masked by black dots. Panels a–c and f–h clearly show that the AO/NAO has a large influence on the variability of the velocity driven FW export anomaly, but that the FW concentration driven FW export anomaly is related to SLP anomalies over the central Arctic. Panels d–e illustrate that FW from Eurasian runoff and Pacific FW has a maximum concentration in Fram Strait during opposite phases of SLP anomalies over the Arctic Ocean.

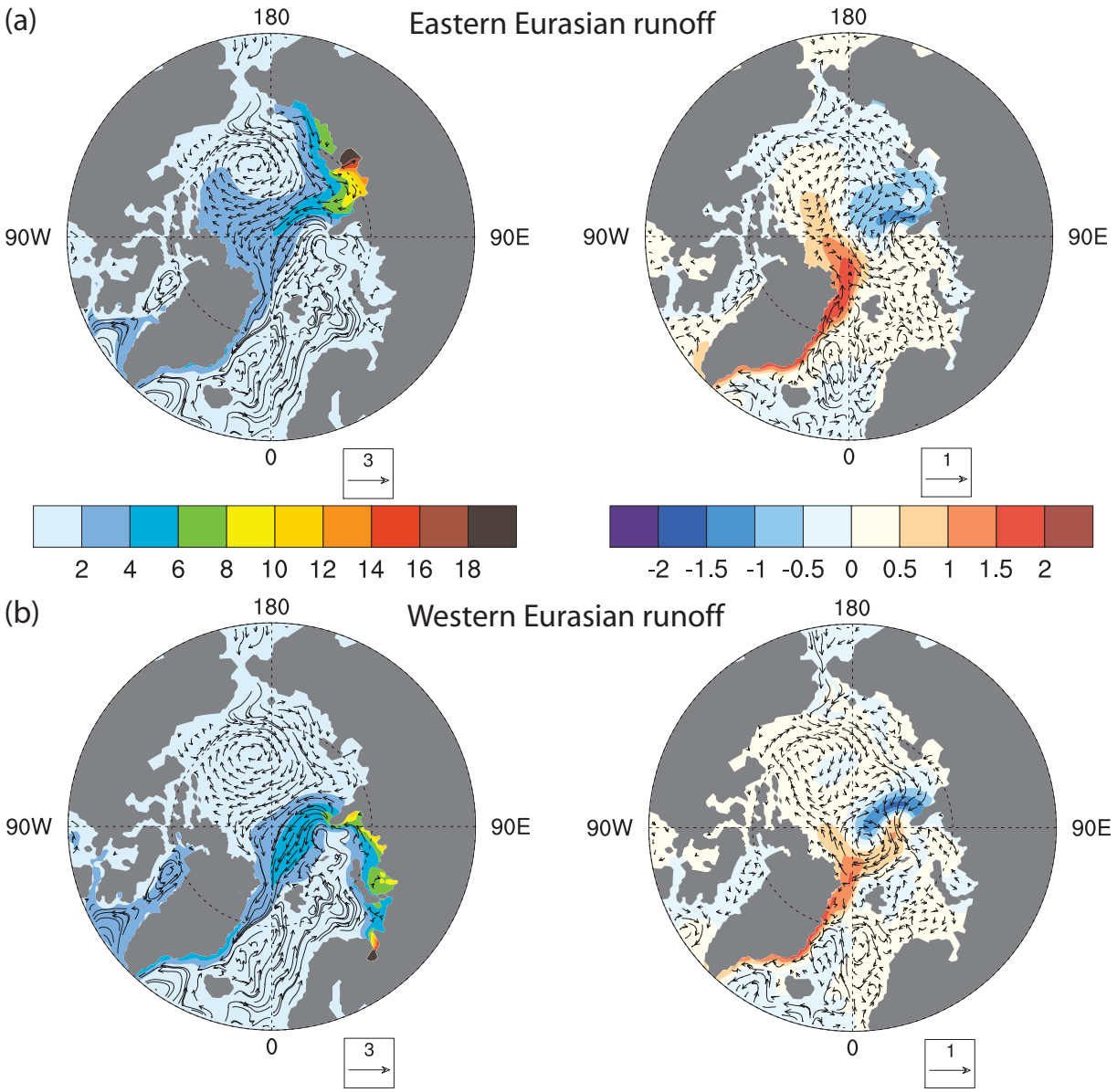

Figure 8. Shown are the mean FW column [m] and velocity [cm/s] in the upper 247 m (left side) over simulation year 440 to 539 and the difference between composites of high and low phases of FW concentration anomalies in Fram Strait (right side) for FW from individual sources (eastern Eurasian river runoff (a), western Eurasian runoff (b), Pacific FW (c), and North American runoff (d)). Red colors in the difference plots indicate that the FW concentration from a given source is increased in that region during periods when the concentration of FW from this source in Fram Strait is high, compared to periods of low concentrations of FW from this source in Fram Strait. Composites are formed from years when FW concentration anomalies in Fram Strait are one standard deviation larger and smaller than the mean. The ocean velocity field is represented by polylines tangent to the instantaneous flow in the neighborhood of the grid point, with a reference vector [cm/s] in the lower right corner. Figure continues on the next page.

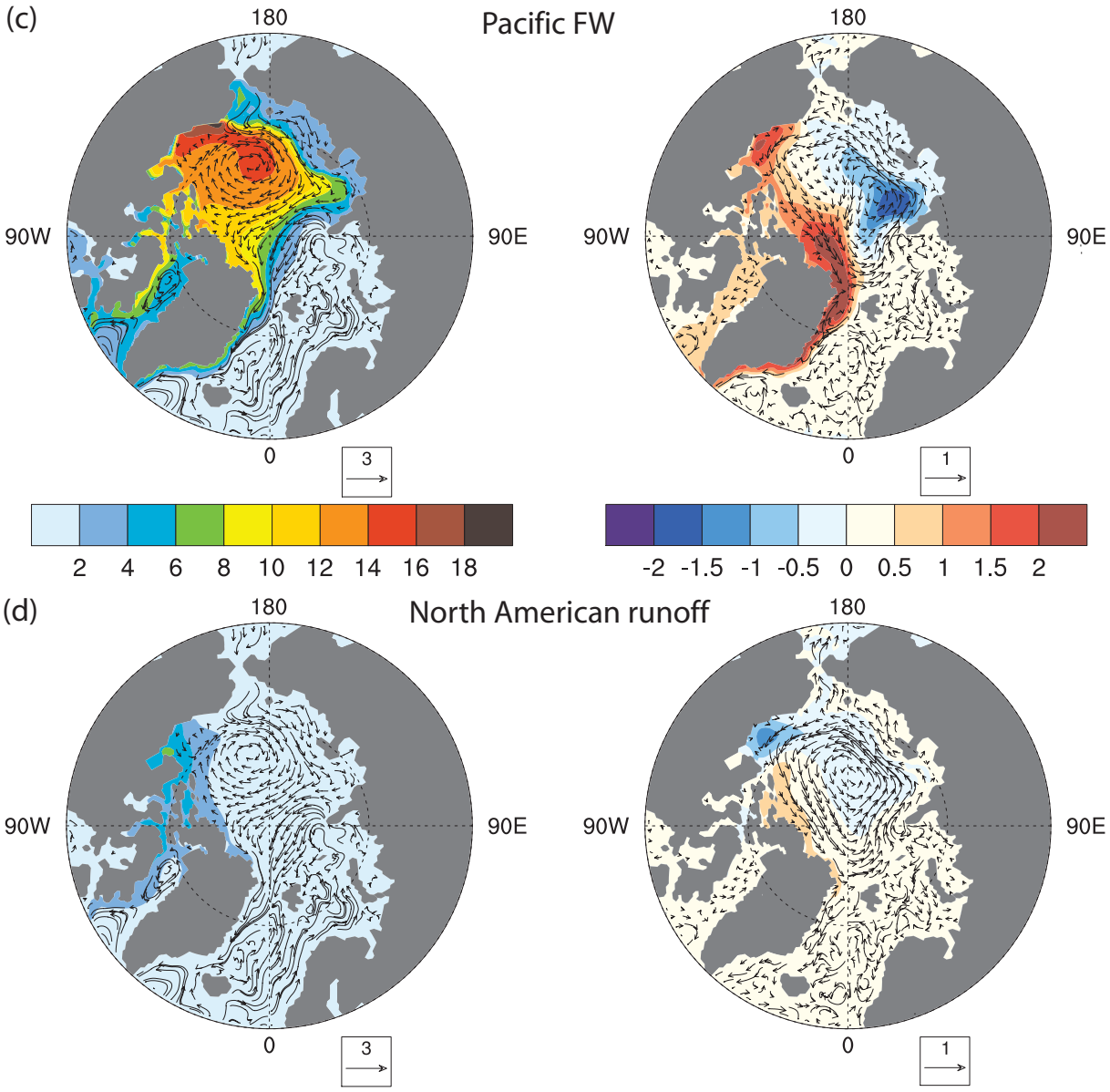

Figure 8. (continued)

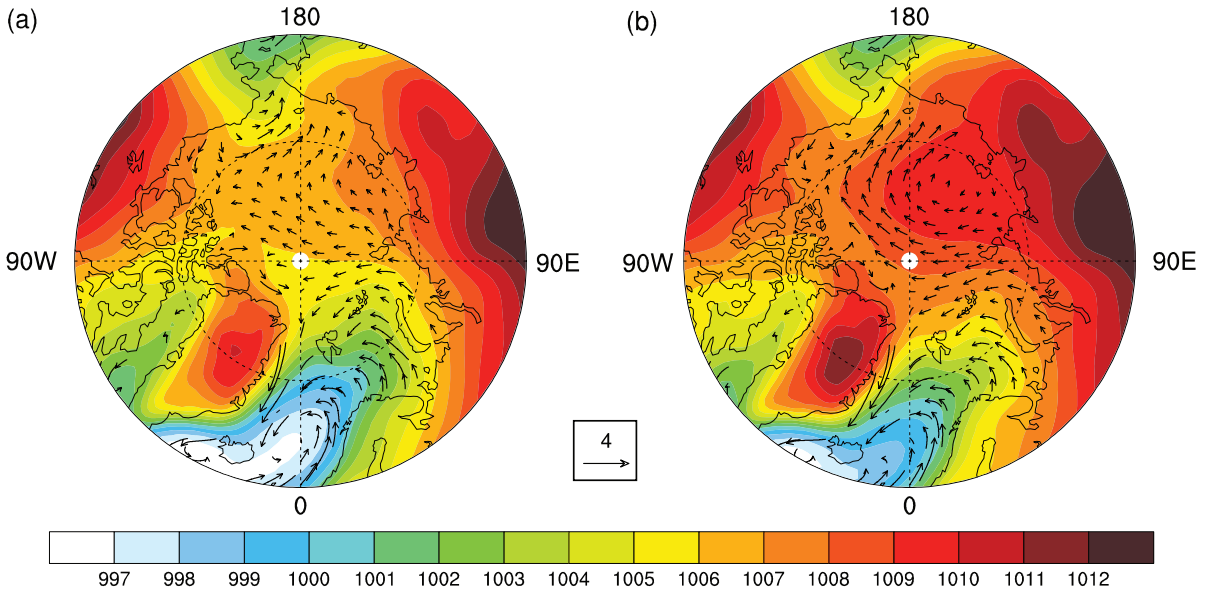

Figure 9. Shown are composites of the simulated SLP pattern (shaded) and 1000 hPa wind [cm/s] over the ocean during (a) positive and (b) negative Vorticity index phases, to indicate the typical SLP pressure pattern associated with different phases of the Vorticity index. Composites are formed from years with a Vorticity index one standard deviation higher and lower than the mean.

Table 4. Maximum correlation of the 3-year running mean Vorticity index with the total Fram Strait FW export, the velocity driven FW export anomaly, and the FW concentration anomaly (total and from different sources), together with the lag [in years] at which they occur. Only correlation coefficients significant at the 95% level or higher are shown.

FW export anomaly	Correlation	Lag [yr]
Total FW export	0.37 & −0.43	0 & 3
Velocity of FW export	−0.34	2
Total FW concentration	0.33 & −0.37	0–1 & 3
Pacific FW concentration	0.64	1
N. American runoff concentration	0.43	1–2
E. Eurasian runoff concentration	−0.35	3
W. Eurasian runoff concentration	−0.35	1–2
NSIM FW concentration	0.45	1
Net precipitation FW concentration	0.43	1

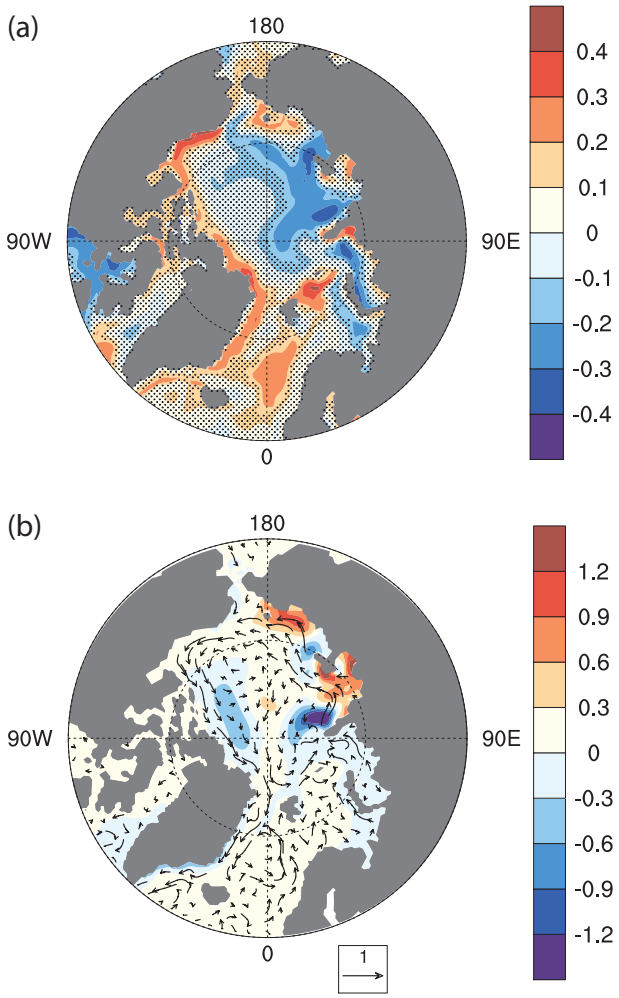

Figure 10. In (a), the correlation between the FW storage in the top 247 m and the annual Vorticity index is shown. Correlations below the 95% significance level are masked by black dots. The dipole pattern in the correlation between the Vorticity index and the FW export leads to different responses of the Eurasian runoff and the Pacific FW to the forcing by the Vorticity index. In (b), a difference plot of the FW column [m] from eastern Eurasian runoff between composites of years with a very positive and very negative annual Vorticity index are shown (composites are formed from years with one standard deviation larger or smaller than the mean). Red (blue) colors indicate regions where more (less) eastern Eurasian runoff is present during positive Vorticity index phases. Hence, this figure shows that during positive Vorticity index phases, the runoff from eastern Eurasia stays on the shelf, whereas during negative Vorticity index phases, the simulated runoff leaves the Eurasian shelf and enters the TDS.

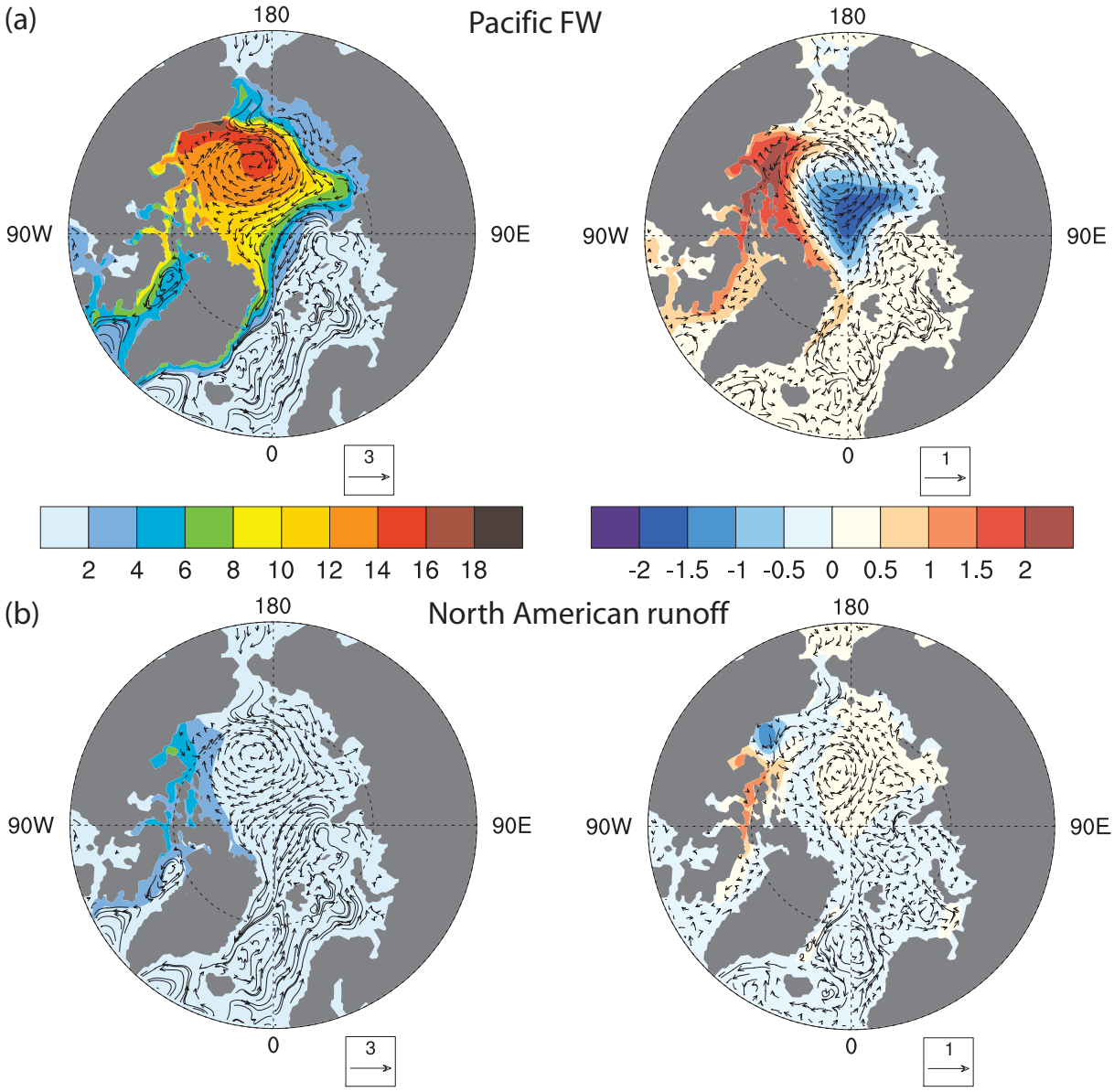

Figure 11. As Fig. 8, but for the FW concentration driven FW export anomalies in the CAA from (a) Pacific FW, (b) North American runoff, (c) eastern and (d) western Eurasian runoff. Figure continues on the next page.

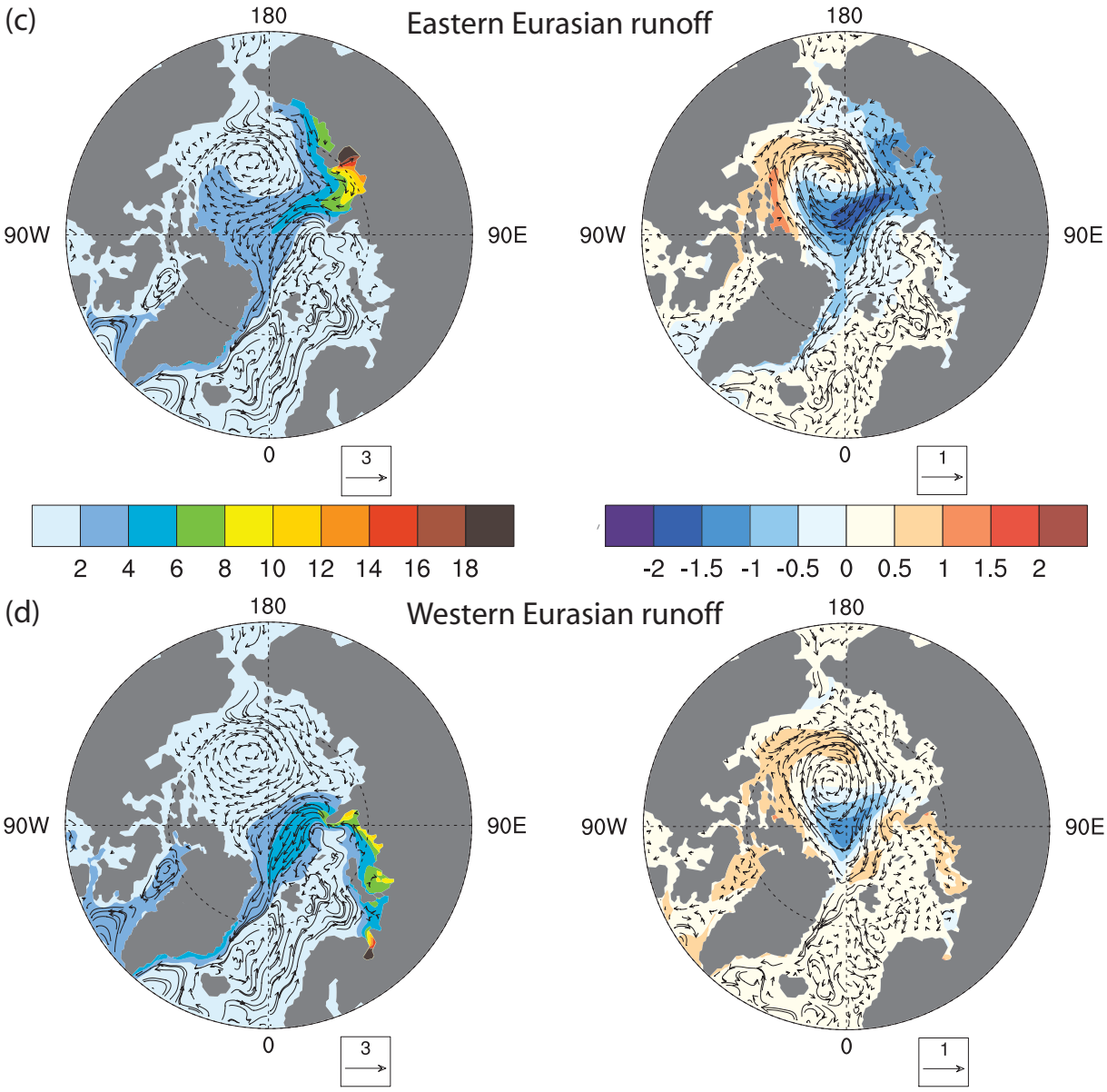

Figure 11. (continued)